Journal of Dynamics, Monitoring and Diagnostics, 2024, 3, 156-177
https://doi.org/10.37965/jdmd.2024.534

ISTP
RESEARCH ARTICLE

Temporally Preserving Latent Variable Models: Offline and Online Training for Reconstruction and Interpretation of Fault Data for Gearbox Condition Monitoring

Ryan Balshaw, P. Stephan Heyns, Daniel N. Wilke, and Stephan Schmidt
Center for Asset Integrity Management, Department of Mechanical and Aeronautical Engineering, University of Pretoria, Pretoria, South Africa

(Received 22 April 2024; Revised 01 June 2024; Accepted 14 June 2024; Published online 17 June 2024)

Abstract: Latent variable models can effectively determine the condition of essential rotating machinery without needing labeled data. These models analyze vibration data via an unsupervised learning strategy. Temporal preservation is necessary to obtain an informative latent manifold for the fault diagnosis task. In a temporal-preserving context, two approaches exist to develop a condition-monitoring methodology: offline and online. For latent variable models, the available training modes are not different. While many traditional methods use offline training, online training can dynamically adjust the latent manifold, possibly leading to better fault signature extraction from the vibration data. This study explores online training using temporal-preserving latent variable models. Within online training, there are two main methods: one focuses on reconstructing data and the other on interpreting the data components. Both are considered to evaluate how they diagnose faults over time. Using two experimental datasets, the study confirms that models from both training modes can detect changes in machinery health and identify faults even under varying conditions. Importantly, the complementarity of offline and online models is emphasized, reassuring their versatility in fault diagnostics. Understanding the implications of the training approach and the available model formulations is crucial for further research in latent variable model-based fault diagnostics.

Keywords: Condition monitoring; unsupervised learning; latent variable models; temporal preservation; training approaches

Abbreviations

BPFO	Ball pass frequency for the outer race
C-AIM	Center for asset integrity management
CCR	Cumulative contribution rate
CD	Condition deviance
CI	Condition interval
CM	Condition monitoring
dB	Decibel
DFT	Discrete Fourier transform
FIR	Finite impulse response
GAN	Generative adversarial network
HI	Health indicator
ICA	Independent component analysis
IMS	Intelligent maintenance systems
LHI	Latent health indicator
LVM	Latent variable model
PCA	Principal component analysis
PD	Path dependent
PI	Path independent
PPCA	Probabilistic principal component analysis
RMS	Root mean square
SASE	Synchronous average of the square envelope
SE	Square envelope
SES	Square envelope spectrum
SMSE	Synchronous median of the square envelope
SNR	Signal-to-noise ratio
SRICA	Spectrally regularized independent component analysis
SSA	Singular spectrum analysis
VAE	Variational auto-encoder

Corresponding author: Ryan Balshaw (e-mail: ryanbalshaw1@gmail.com).

I. INTRODUCTION

Condition monitoring (CM) is essential for proactively managing and maintaining critical industrial assets, such as wind turbines and ball mills, where downtime can induce significant operational losses [1–3]. Decreased asset performance impacted by changes in an asset's instantaneous health condition requires interventions driven by machine CM approaches [4–6]. Inferring the condition of rotating machinery is achieved through informative CM data that capture deviations in the internal health state [7]. Common CM data include temperature measurements [8,9], acoustic measurements [10,11], oil lubricant measurements [12,13], vibration measurements [14,15], and multi-sensor measurements [16,17].

Among such measurement types, vibration data provide an instantaneous asset representation useful for capturing cyclic phenomena and serve as a robust basis for capturing fault signatures representative of rotating machinery [3,15,18]. Hence, vibration-based approaches are prominent for gearbox CM [5,19].

Within vibration-based CM, signal processing and learning-based methodologies represent two distinct domains of active academic and industrial practitioner interest [20]. Such methodologies, in principle, enable CM by facilitating a transformation of the raw vibration data

into a diagnostic-rich representation to guide maintenance decision-making. This is achieved through health indicators (HIs), which must contain enhanced diagnostic information to improve the CM process. Effective HIs enable effective fault diagnosis and prognosis [4,21,22]. Therefore, developing or extracting relevant HIs is crucial. A general workflow of vibration-based CM is present in Fig. 1. The CM workflow presented in Fig. 1 identifies the multiple stages contained within the CM life cycle. First, vibration data are measured and stored for an asset using sensors. Then, HIs are constructed to enable accurate fault diagnosis and prognosis. Finally, informed maintenance decisions are made based on actional insights gleaned from the diagnosis and prognosis steps.

For vibration-based CM, signal processing methodologies develop HIs by enhancing the prevalence of fault signatures nested within vibration data. This is achieved through time domain indicators [18,23], time-frequency analysis [24–27], spectral analysis [5,28], cyclostationary analysis [29,30], or signal enhancement strategies [31–34]. Conversely, learning-based methodologies use statistical, machine, and deep learning-based approaches to accomplish CM [21]. In general, learning-based methods offload the complexity of fault signature enhancement to a model to perform fault diagnosis and prognosis [4,21].

In conventional CM applications, learning-based models are applied in various learning settings: *(i)* supervised learning [35–37], *(ii)* transfer learning [38–41], and *(iii)* unsupervised learning [42,43]. Supervised learning is a popular learning-based setting used to automatically identify fault signatures to classify different potential fault states, e.g., Huang *et al.* [44].

For a supervised learning approach, data labeling is a restrictive requirement [21,45]. Unsupervised learning approaches, e.g., latent variable models (LVMs), can perform CM without labeled fault data [20,21,45]. These approaches capture intrinsic vibration data representations and are used for downstream health state monitoring tasks, e.g., Booyse *et al.* [42]. Feature extraction, as highlighted in Fig. 1, is performed by the LVM to further automate the detection of fault signatures [42]. Conventionally, vibration-based CM with LVMs uses temporal non-preserving approaches, i.e., where the time within the sensor is collapsed, and only record time, i.e., the chronological order of the recorded vibration data, is preserved [43]. Moreover, data reconstruction-based techniques can only be used to perform LVM-based anomaly detection to detect asset health state deviations [45]. Hence, a temporally non-preserving setting restricts the pertinence of LVMs in vibration-based CM and limits LVMs to anomaly detection operations [45]. Encouragingly, recent advancements demonstrate the importance of temporal preservation in enhancing LVM interpretability, which is essential to enable effective anomaly detection and fault diagnosis when using LVMs [43]. Temporal preservation ensures that the temporal characteristics of the vibration data are preserved in the extracted HIs, enabling both increased analysis flexibility from the additional time structure and the use of the latent manifold for CM. This increased capacity to detect damage, isolate the fault condition, and perform fault trending encapsulates the elements of fault diagnosis [6,43,46]. Furthermore, temporal preservation leads to latent health indicators (LHIs) that better characterize fault signature mechanisms in the LVM latent manifold [47].

In this study, two LVM training approaches are contrasted – offline and online. These approaches are contrasted in their ability to extract HIs that can be used in CM applications. The offline training approach involves static model parameter estimation from historical vibration data [42,43,47] by assuming and using an existing historical healthy dataset [42,48,49]. Alternatively, the online training approach dynamically adjusts the model parameters in real time, potentially enhancing fault diagnostics through continuous model adaptation. Moreover, offline training decouples the model estimation and data evaluation step, while online training performs both simultaneously. Importantly, online training is foundational to many signal processing strategies, e.g., blind deconvolution [34,50], band demodulation [33,51,52], and online monitoring [53,54], but is less common in LVM-based CM applications. Hence, this investigation studies these training strategies' efficacy. Particularly, this work focuses on how different training approaches impact the latent manifold's utility for CM. Consequently, we consider and investigate a CM scenario where the distribution of the healthy data is not known a priori through a reference dataset. This comparative analysis will reveal which training approach better captures data fault signatures essential for accurate LVM-based CM. The context of this study within the vibration-based CM workflow is captured in Fig. 1.

To facilitate a comparison between LVM training approaches, this study employs a probabilistic principal component analysis (PPCA) model [47,55], referred to as the PPCA_h model, to represent offline LVMs trained on assumed healthy, historical data. In contrast, online training examines the evolution of intrinsic data features through record time. This makes it possible to use and apply a new class of LVM algorithms. Two domains for LVMs are considered in this work: *(i)* reconstruction-focused LVMs, which aim to maximize the variance explained in observed vibration data via latent decompositions that capture variance-centric data components [42,56–58], and *(ii)*

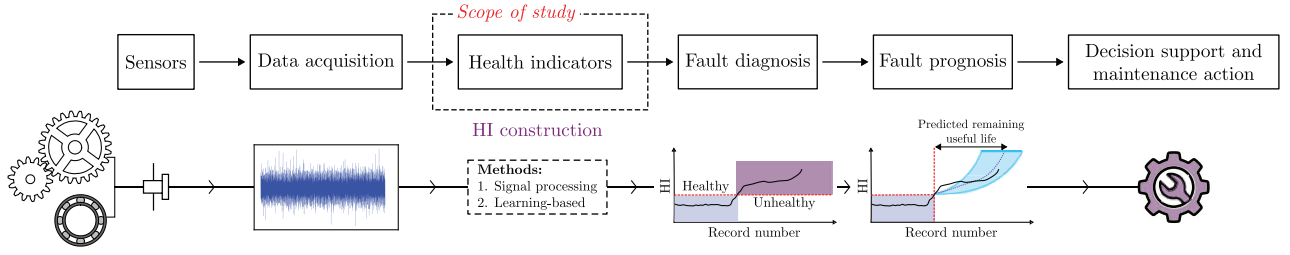

Fig. 1. A general overview of the vibration-based CM workflow from the sensors that record the vibration data to the final maintenance decision-making step. The position of this study is demonstrated within this workflow. Learning-based methods for HI construction are considered in this study.

interpretation-focused LVMs, which seek an informative latent manifold driven by statistical independence and non-Gaussianity [56,59–61]. Note that the PPCA$_h$ model is considered a reconstruction-focused LVM.

LVMs from both domains seek an informative latent manifold but measure informativeness uniquely. More specifically, reconstruction-focused models seek a latent manifold to maximize the variance captured within the observed data. Alternatively, interpretation-focused models seek to recover the underlying components in the original vibration data. This provides a level of interpretability whereby these models aim to recover components contributing to the original signal. Recovering the original components enables the interpretation of these components' characteristics and potential sources. This is suitable for vibration data from rotating machinery as the vibrations from different components are typically additive [62]. In the online training approach, considering reconstruction-focused and interpretation-focused LVMs is crucial, as maximal variance does not always equate to the most informative fault signature extraction strategy. Furthermore, non-Gaussianity, a key property in signal processing for signal enhancement, has attracted much attention for its effectiveness in detecting damage in rotating machinery [15,34,63].

The consideration and context of temporal-preserving LVMs in vibration-based CM for this study are demonstrated in Fig. 2. The LVM encoder and decoder operate as latent feature extractors and reconstructors. From the two feature spaces produced by these two LVM components, i.e., the latent manifold and the reconstructed vibration data, respectively, LHIs and HIs can be computed [42,47]. This study uses these LHIs and HIs to contrast offline and online temporal-preserving LVMs. For LVMs developed using offline or online training, only one training approach is applied to a given LVM. Figure 2 demonstrates that offline LVMs are implemented using a historical dataset, while online LVMs iteratively update the encoder and decoder parameters for each observed vibration signal. To enable the comparison of the considered offline and online LVMs in a fault diagnosis setting, temporal preservation is used [43]. Temporal preservation yields informative indicators by preserving sensor time, thereby enhancing both the indicators and the LVM analysis setting. This produces HIs and LHIs with a time dependency, as demonstrated in Fig. 2.

Various approaches related to offline and online LVMs have been used in the literature. In the domain of offline training, Booyse *et al.* [10] demonstrated the practicality of two reconstruction-focused LVMs in an offline setting, namely generative adversarial networks (GANs) [64] and variational auto-encoders (VAEs) [58] in the anomaly detection setting. Alternative LVM formulations have been considered by Hu *et al.* [65], while Marx and Gryllias [66] investigated the implications of incorporating prior failure information using a numerical supplementation approach to introduce augmented failure data.

In the online training domain for reconstruction-focused methods, prominent interest has been placed in using singular spectrum analysis (SSA) techniques to decompose a Hankel matrix of vibration data into a sum of variance-weighted rank-one matrices [67]. The SSA decomposition process is variance-driven [68] and strongly correlates with signal processing theory [69,70]. Recent works, e.g., [71–73], have explored and developed methodologies to improve the adoption of variance-based decomposition processes in vibration-based CM. In the online training domain for interpretation-focused methods, ICA-based procedures, e.g., [74], are prevalent and have been demonstrated to extract signal information with abundant fault diagnostic information.

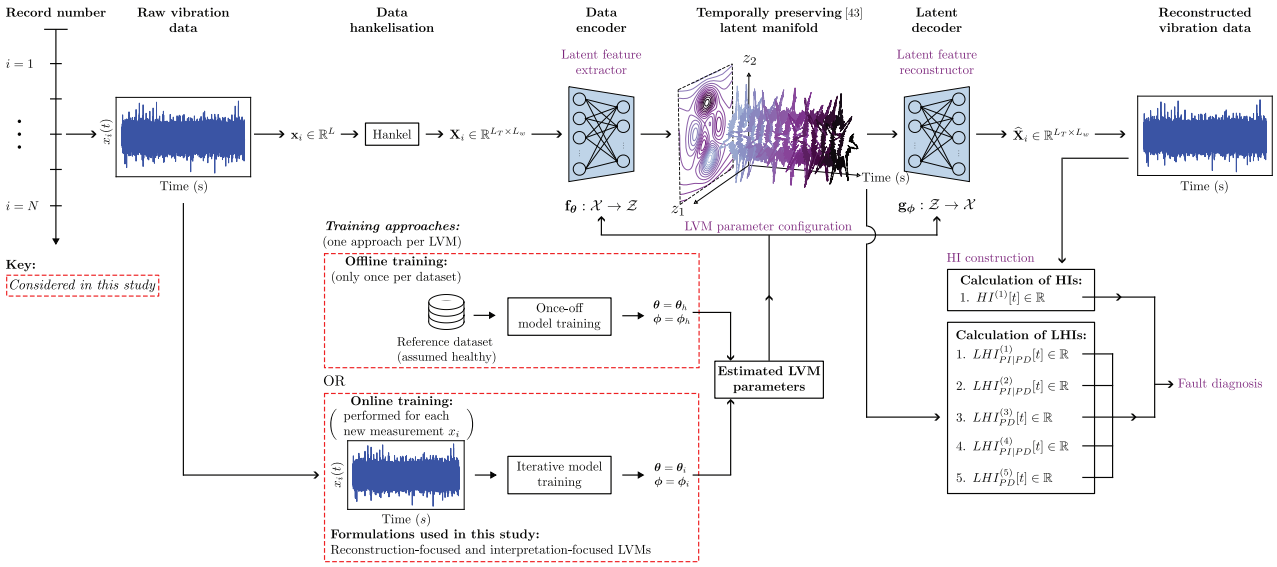

Fig. 2. The temporally preserved LVM-based pipeline used to extract HIs and LHIs for vibration-based CM applications. Note that the latent manifold is set to $\mathbb{R}^2$ with an explicitly disentangled time variable t, i.e., sensor time. Temporal preservation ensures that the HIs and LHIs are functions of sensor time. The LVM training approach, i.e., the LVM implementation procedure, directly affects the LVM parameters ($\boldsymbol{\theta}$ and $\boldsymbol{\phi}$) of the data encoder $f_{\boldsymbol{\theta}}$ and the latent decoder $g_{\boldsymbol{\phi}}$, respectively. One of two training approaches is applied to LVMs: offline or online. For offline training, the parameters are estimated using a reference healthy dataset. In contrast, online training iteratively estimates the LVM parameters using the i^{th} vibration data record. We reserve the subscript of the variable h for the offline training approach and the variable i specifically for the dependency on record time in the online training approach to simplify the notation in this document. All variable notations are clarified in Section II.

In this work, PPCA is used as an online reconstruction-focused LVM, while an independent component analysis (ICA)-based methodology [60,75,76], particularly spectrally regularized ICA (SRICA) [77], which incorporates spectral regularization to avoid duplication of latent information, exemplifies online interpretation-focused models. These models are pivotal in computing LHIs from the latent manifold [47], with LHI quality hinging on the manifold's ability to represent fault signatures. This study contrasts these online LVMs with the offline PPCA_h model to evaluate the impact of LVM formulations on fault diagnosis effectiveness. The research contributes by:

1. Comparing temporally preserving reconstruction-focused and interpretation-focused LVMs for HI extraction in CM applications.
2. Critically assessing the implications of various LVM training approaches, highlighting the complementary nature and utility of online settings for CM.
3. Utilizing two experimental datasets with different fault signatures to demonstrate the complementary strengths and weaknesses of both offline and online LVMs.

The layout of this paper is as follows: Section II elaborates on the considered LVM formulations and constructed HIs within the context of vibration-based CM. A comparative evaluation using a bearing fault dataset follows in Section III, which is paralleled by an analogous analysis using a gear fault dataset in Section IV. Finally, Section V draws conclusions using the findings from Sections III and IV, and gives recommendations for future work.

II. LATENT VARIABLE METHODS

In this section, the principal LVM methodologies used in this work are discussed, all data pre-processing steps are given, and the HIs and LHIs used are described. Focus is given to the form of the offline and online reconstruction-focused LVMs and the online interpretation-focused LVM.

A. BACKGROUND

LVMs represent a probabilistic framework which describes the data distribution $p(\boldsymbol{x})$, where $\boldsymbol{x} \in \mathcal{X} \subset \mathbb{R}^D$, using some unobserved latent variables $\boldsymbol{z} \in \mathcal{Z} \subset \mathbb{R}^d$, where $d \leq D$. The marginal distribution $p(\boldsymbol{x})$, often referred to as the model evidence, is given by

$$p(\boldsymbol{x}) = \int_{\boldsymbol{z}} p(\boldsymbol{x},\boldsymbol{z}) d\boldsymbol{z}. \tag{1}$$

In common LVM applications, the joint distribution $p(\boldsymbol{x},\boldsymbol{z})$ is assumed to factorize

$$p(\boldsymbol{x},\boldsymbol{z}) = p(\boldsymbol{x}|\boldsymbol{z})p(\boldsymbol{z}), \tag{2}$$

where $p(\boldsymbol{x}|\boldsymbol{z})$ is the conditional generative distribution and $p(\boldsymbol{z})$ is a prior distribution over $\boldsymbol{z}$. To infer the posterior distribution $p(\boldsymbol{z}|\boldsymbol{x})$ for the latent variables given some observed data, Bayes' rule is used

$$p(\boldsymbol{z}|\boldsymbol{x}) = \frac{p(\boldsymbol{x}|\boldsymbol{z})p(\boldsymbol{z})}{p(\boldsymbol{x})}. \tag{3}$$

Different strategies represent the LVM formulation, each constituting a unique interpretation of the general LVM objective. Typically, an encoding transition function $\boldsymbol{f_\theta}: \boldsymbol{\chi} \rightarrow \boldsymbol{z}$ and a decoding transition function $\boldsymbol{g_\phi}: \boldsymbol{z} \rightarrow \boldsymbol{\chi}$ are used to parametrize the mapping from $\boldsymbol{x}$ to $\boldsymbol{z}$ and vice versa. These functions represent the transfer of information between the data space and the latent manifold, and the parameters of these functions are estimated to allow the LVM to generate data and capture the intrinsic properties in the data [57]. This work develops and investigates encoding and decoding transition functions for offline or online training approaches, as demonstrated in Fig. 2. Thus, they depend on a reference dataset or record time and are denoted by $\boldsymbol{f_{\theta_h}}$ and $\boldsymbol{g_{\phi_h}}$ or by $\boldsymbol{f_{\theta_i}}$ and $\boldsymbol{g_{\phi_i}}$, respectively.

In the domain of LVMs, there are two primary formulations: explicit and implicit. In explicit LVM formulations, assumptions are made regarding the form of the distribution of interest for explicit parametrization, e.g., PPCA [55], which assumes linear Gaussian distributions, or VAEs [58], which assume nonlinear Gaussian distributions. Note that the linearity of the model refers to the parametrization of the encoding and decoding transition functions used for mapping from $\boldsymbol{x}$ and $\boldsymbol{z}$ and vice versa, not the form of the chosen distribution. In implicit LVM formulations, a stochastic procedure is defined to generate data and no distribution assumptions are directly made except for the form of the prior $p(\boldsymbol{z})$, e.g., GANs [64,78]. Typically, LVMs are reconstruction-focused, whereby they are primarily concerned with sample generation, and work has been done to improve the performance of these models [79–83].

In this work, two linear LVM formulations represent methods from the reconstruction-focused and interpretation-focused LVM. Thus, the encoding and decoding transition functions represent an affine linear function. For the considered LVMs, both transition functions are available to ensure that the latent manifold and the reconstructed data space are accessible. Each technique will be briefly discussed in turn.

B. RECONSTRUCTION-FOCUSED LVMS

The first LVM used in this work is PPCA, wherein principal component analysis (PCA) operates as a maximum likelihood solution for the LVM formulation [57]. This model is used as the reconstruction-focused LVM developed using both offline and online training. For the PPCA model, the prior distribution is assumed to be $p(\boldsymbol{z}) = \mathcal{N}(\boldsymbol{z}|\boldsymbol{0},\boldsymbol{I})$, represents an isotropic Gaussian distribution. The generative process for PPCA is expressed as

$$\boldsymbol{x} = \boldsymbol{W}\boldsymbol{z} + \boldsymbol{\mu_x} + \boldsymbol{\epsilon}, \tag{4}$$

where $\boldsymbol{\mu_x}$ represents the first moment of $\boldsymbol{x}$, and $\boldsymbol{\epsilon} \sim \mathcal{N}(\boldsymbol{\epsilon}|\boldsymbol{0}, \sigma \cdot \boldsymbol{I})$ is a zero-mean isotropic Gaussian variable. Equation (4) implies that the generative distribution $p(\boldsymbol{x}|\boldsymbol{z})$ follows a Gaussian distribution. The posterior distribution $p(\boldsymbol{z}|\boldsymbol{x})$ for the PPCA model is given by

$$p(\boldsymbol{z}|\boldsymbol{x}) = \mathcal{N}(\boldsymbol{z}|\boldsymbol{M}^{-1}\boldsymbol{W}^T(\boldsymbol{x}-\boldsymbol{\mu_x}), \sigma^{-2}\boldsymbol{M}), \tag{5}$$

where $\boldsymbol{M} = \boldsymbol{W}^T\boldsymbol{W} + \sigma^2 \cdot \boldsymbol{I}$. The maximum likelihood solution for $\boldsymbol{W}$ and σ^2, presented in Ref. [55], shows the latent encoding transformation as

$$\boldsymbol{z} = \text{diag}\left(\frac{\sqrt{\lambda_1 - \sigma^2}}{\lambda_1}, \cdots, \frac{\sqrt{\lambda_d - \sigma^2}}{\lambda_d}\right)\boldsymbol{U}_d^T(\boldsymbol{x}-\boldsymbol{\mu_x}), \tag{6}$$

where $\boldsymbol{U}_d \in \mathbb{R}^{D\times d} = [\boldsymbol{u}_1, \cdots, \boldsymbol{u}_d]$ represents the eigenvector matrix of the covariance matrix $\boldsymbol{C} = E_{\boldsymbol{x}\sim p(\boldsymbol{x})}\{\boldsymbol{x}\boldsymbol{x}^T\}$ arranged in descending order based on the eigenvalues

(λ) of $\boldsymbol{C}$. Equation (6) represents the mean of $p(\boldsymbol{z}|\boldsymbol{x})$ and can be identified as a scaled version of the PCA latent transformation $\boldsymbol{z} = \boldsymbol{U}_d^T(\boldsymbol{x} - \boldsymbol{\mu}_{\boldsymbol{x}})$ [57]. In the offline training scenario, the PPCA$_h$ model parameters are obtained using a reference set of observed vibration data signals. For the online training approach, the PPCA model parameters are obtained for each sequentially ordered vibration signal $x_i(t)$, $i \in [1,N]$. The offline PPCA$_h$ model is used as a baseline to evaluate the performance of the online LVMs. This comparison is necessary to evaluate the implications of online training in an LVM-based fault diagnostics context.

C. INTERPRETATION-FOCUSED LVMS

The second LVM used in this work is an ICA methodology based on the negentropy-based ICA formulation proposed in Hyvärinen [38]. This model is used as the interpretation-focused LVM and is developed using online training. The noiseless ICA generative model is given by

$$\boldsymbol{x} = \boldsymbol{A}\boldsymbol{z}, \tag{7}$$

where $\boldsymbol{A} \in \mathbb{R}^{D\times d}$. In this ICA formulation, the latent variables are enforced to be independent, i.e.,

$$p(\boldsymbol{z}) = \prod_{j=1}^{d} p(z_j), \tag{8}$$

and the latent variables are assumed to be non-Gaussian [75]. Statistical independence implies that the individual latent variables are maximally informative, i.e., provide no useful information to other latent variables. The encoding transformation to obtain the latent variables is represented by

$$\boldsymbol{z} = \boldsymbol{W}\boldsymbol{x}, \tag{9}$$

where $\boldsymbol{W} \in \mathbb{R}^{d\times D} = [\boldsymbol{w}_1, \cdots, \boldsymbol{w}_d]^T$ represents a matrix of component vectors. Conventionally, A is unknown, and ICA methodologies exploit proxy criteria to represent the ICA transform without assuming the probabilistic form of the generative model [75]. A popular ICA methodology uses an approximation of negentropy [84] as a measure of non-Gaussianity to estimate the ICA model parameters. Non-Gaussianity is a key requirement to enforce statistical independence and obtain proxy measures for the latent manifold features to guide the LVM parameter estimation process. The aversion towards Gaussianity for interpretation-focused methods is readily motivated by the affine property of an isotropic Gaussian distribution [57]. From this property, it may be impossible to distinguish between latent variables that deviate by a simple latent transformation, e.g., a rotation, which produces infinitely many combinations of Gaussian latent variables that satisfy the independence property [57].

In Ref. [77], the issue of source duplication in single-channel time-series applications, discussed in the work of Hyvärinen [36] and Davies and James [42], is addressed via the addition of a spectral regularization term which enforces the spectral representations of the vectors in $\boldsymbol{W}$ to be orthogonal. The methodology from Ref. [77] uses a regularized optimization algorithm applied to the negentropy approximations from Ref. [84] to estimate the SRICA model parameters. The non-quadratic exponential function is used in this work to approximate negentropy as it is a robust estimator [60,75].

In this work, the SRICA model is used to represent an interpretation-focused LVM developed using the online training approach and is compared to PPCA within the context of the online training approach and to the PPCA$_h$ model in the context of the offline training approach. The data pre-processing steps used in this work are discussed in the following section. Appendix A establishes an important connection between the considered LVM models and existing signal processing literature.

D. DATA PROCESSING

Given a signal $x_i[n]$, where $n \subset Z^+ = \{1, \cdots, L\}$ and L is the length of the signal, an initial pre-processing step is required to represent the raw vibration signal, which enables LVM model parameter estimation for LVM-based CM. In this work, a data Hankelization step, sometimes referred to as a truncated Toeplitz matrix, is used to obtain a Hankel matrix

$$\boldsymbol{X}_i = \begin{bmatrix} x_i[1] & \cdots & x_i[L_w] \\ x_i[L_{sft}] & \cdots & x_i[L_{sft} + L_w] \\ x_i[2 \cdot L_{sft}] & \cdots & x_i[2 \cdot L_{sft} + L_w] \\ \vdots & \ddots & \vdots \\ x_i[L_{sft} \cdot (L_T - 1)] & \cdots & x_i[L_{sft} \cdot (L_T - 1) + L_w] \end{bmatrix}, \tag{10}$$

where L_w is the window length, L_{sft} is the shift parameter, and $L_T = \left\lfloor \frac{L_w}{L_{sft}} \right\rfloor + 1$ represents the number of rows in $\boldsymbol{X}_i \in \mathbb{R}^{L_T \times L_w}$ [42,47]. The rows of $\boldsymbol{X}_i$ represent samples of the data vector $\boldsymbol{x} \in \mathbb{R}^{L_w}$, i.e., $D = L_w$. The pre-processing steps required for LVMs developed under the offline training approach are discussed in Ref. [47]. The pre-processing steps related to the online training approach are discussed in this section. After the Hankelization step, a standard pre-processing strategy is to center the columns of $\boldsymbol{X}_i$, ensuring that the components of $\boldsymbol{x}$ are zero-mean. This is given by

$$\bar{\boldsymbol{X}}_i = \boldsymbol{X}_i - \boldsymbol{1}\boldsymbol{\mu}_i^T, \tag{11}$$

where $\boldsymbol{\mu}_i \in \mathbb{R}^{L_w}$ is a column vector of the feature-wise means of $\boldsymbol{X}_i$ and $\boldsymbol{1} \in \mathbb{R}^{L_w}$ is a constant vector with elements 1 [47]. Note that the data is not standardized in this work as standardization coupled with online training may remove any inter-record variance useful for condition inference. For the SRICA methodology, a pre-whitening step is used to pre-process the data matrix $\bar{\boldsymbol{X}}_i$ further. Pre-whitening is a useful processing step to reduce the approximation complexity required to obtain the vectors $\boldsymbol{w}$ of the independent component matrix $\boldsymbol{W}$ [59]. Pre-whitening is a pre-processing strategy that removes any second-order correlations in $\bar{\boldsymbol{X}}_i$ and is given by a linear transformation via

$$\tilde{\mathrm{x}} = \mathbf{U}_\mathrm{D}\mathbf{L}_\mathrm{D}^{-1/2}\mathbf{U}_\mathrm{D}^\mathrm{T}\bar{\mathbf{X}}, \tag{12}$$

where $\bar{\boldsymbol{x}} \in \mathbb{R}^{L_w}$ is a column vector stored in the rows of $\bar{\boldsymbol{X}}_i$, $\tilde{\boldsymbol{x}} \in \mathbb{R}^{L_w}$ is the whitened variable, $\boldsymbol{U}_D \in \mathbb{R}^{L_w \times L_w}$ is the full rank eigenvector matrix of the data covariance matrix $\boldsymbol{C}_i = E\{\bar{\boldsymbol{x}}\bar{\boldsymbol{x}}^T\}$ [57], and $\boldsymbol{L}_D^{-1/2} \in \mathbb{R}^{L_w \times L_w} = \mathrm{diag}(\lambda_1^{-1/2}, \cdots, \lambda_{L_w}^{-1/2})$ is a diagonal matrix of the inverse square root of the eigenvalues λ from $\boldsymbol{C}$. To enable fault diagnostics for the interpretation-focused LVM, the implications of the pre-whitening step must be accounted for, as this limits the ability to perform fault trending through record time. The

implication of pre-whitening is discussed in Ref. [59]. PPCA has no such issue as the centering process given in Equation (11) does not remove any scale variations in the data. In this work, we use a simple re-scaling of the latent components for the interpretation-focused LVM via the latent kurtosis, i.e.,

$$z = \text{diag}(\sqrt{\text{kurt}(z_1)}, \cdots, \sqrt{\text{kurt}(z_d)})\boldsymbol{W}\tilde{\boldsymbol{x}}, \tag{13}$$

where kurt$(\cdot)$ represents the sample kurtosis. This re-scaling ensures that the prominence of specific underlying features in the latent manifold can be compared through record time. The use of the square root was made based on its usage in signal processing works, e.g., Ref. [85], and in our investigations, we found that this scaling gave better results. The choice of scaling used is not proposed to be optimal and may require further research. The optimization of the scaling function is outside the scope of this work.

E. LATENT HEALTH INDICATORS

A transformation of the latent and reconstructed data space is required for CM purposes to infer the condition of the asset of interest based on a sequential set of vibration signals [47]. This work uses a simple set of statistical distance-based LHIs from Ref. [47]. The dissimilarity-based sub-class is used in this work as it requires no access to healthy latent manifold representations, and the metrics are simple to calculate. The subset of LHIs used was selected from a broader range of potential indicators for temporal-preserving LVMs. This approach enables this work to maintain a focused investigation and refine our analysis. A more comprehensive exploration of HIs and LHIs will be pursued in future research. The first HI is the reconstruction error

$$HI^{(1)}[t] = \frac{1}{D} \cdot \|\boldsymbol{x}_t - \hat{\boldsymbol{x}}_t\|_2^2, \tag{14}$$

which represents the mean squared error between the data sample $\boldsymbol{x}_t$ and its reconstruction $\hat{\boldsymbol{x}}_t$. Note that the variable $t \in [0, L_T - 1]$ refers to an integer representation of the sensor time captured by the signal segments in the data Hankelization step discussed in Section II.D and $HI^{(1)}[t] \in \mathbb{R}$ is a scalar. Temporal preservation exploits this sensor time to enhance the information obtained for the condition inference task [43]. The first LHI considered in this work is the normalized Euclidean distance indicator given by

$$LHI^{(1)}_{PI|PD}[t] = \frac{1}{d} \cdot \|z_{t+1} - z_t\|_2, \tag{15}$$

where the path-independent (PI) and path-dependent (PD) latent manifold inference settings capture different latent manifold deviation mechanisms [47], $z_t = 0$ in the PI setting, and d is the dimensionality of z. Sensor time-independent LHIs are identified as PI, while sensor time-dependent LHIs are identified as PD. For LVMs developed using the offline training approach, the dimensionality of the latent manifold is constant and denoted as $d = d_h$. For LVMs developed using the online training approach, the latent manifold may be a function of the observed vibration data and is denoted as $d = d_i$. The second LHI considered in this work is the normalized Manhattan distance

$$LHI^{(2)}_{PI|PD}[t] = \frac{1}{d} \cdot \|z_{t+1} - z_t\|_1, \tag{16}$$

which evaluates the L_1 norm. The third LHI considered in this work is the normalized Canberra distance

$$LHI^{(3)}_{PD}[t] = \frac{1}{d} \cdot \sum_{j=1}^{d} \frac{|z_{t+1,j} - z_{t,j}|}{|z_{t+1,j}| + |z_{t,j}|}, \tag{17}$$

which represents a weighted version of Equation (16). The fourth LHI considered in this work is

$$LHI^{(4)}_{PI|PD}[t] = \frac{1}{d} \cdot \|z_{t+1} - z_t\|_\infty, \tag{18}$$

which represents the normalized Chebyshev distance or uniform norm $\|\cdot\|_\infty$. The final LHI considered in this work is the cosine distance

$$LHI^{(5)}_{PD}[t] = \frac{1}{d} \cdot \cos^{-1}\left(\frac{z_{t+1}^T z_t}{\|z_{t+1}\|_2 \cdot \|z_t\|_2}\right), \tag{19}$$

which represents a latent dimensionality normalized LHI in a non-Euclidean coordinate system [47]. Note that all latent indicators are scalars through sensor time, i.e., $LHI^{(1-5)}_{PI|PD}[t] \in \mathbb{R}$. The $HI^{(1)}[t]$ and $LHI^{(1-5)}_{PI|PD}[t]$ metrics are used to infer the instantaneous asset health condition and represent deviations in the data space and the latent manifold in the presence of some fault condition. For the remainder of this study, the notation identifying the dependence on sensor time t is dropped for all HIs and LHIs for brevity.

III. EXPERIMENTAL BEARING DATASET STUDY

This work uses two experimental datasets representing different gearbox failure mechanisms and operating condition states to compare the offline and online LVMs. The first considered dataset is an experimental bearing fault dataset with constant operating conditions. For this investigation, the properties of interest are the ability of the considered HIs and LHIs to detect and trend the damage and localize the faulty component of interest, i.e., to perform fault diagnosis [6,86]. This comparison approach serves to fully understand the implications of the choice of training approach and LVM formulation without proposing a method to use the multiple HIs simultaneously for fault diagnosis. We leave the investigation potential of the full CM problem for future work.

The experimental setup for the first dataset is outlined in Section III.A, followed by the LVM specifications in Section III.B. Section III.C details the diagnostic metrics used to evaluate and compare the HIs and LHIs from the considered LVMs. The results of the first experimental dataset are presented in Section III.D.

A. BEARING STUDY: EXPERIMENTAL SETUP

The first experimental dataset considered is one made available by the NSF I/UCR Center for Intelligent Maintenance Systems (IMS) [87]. The dataset consists of bearing housing accelerometer data captured for three run-to-failure endurance tests. The raw vibration data corresponding to the first bearing of the second run-to-failure endurance test is investigated in this work.

A schematic of the experimental setup is depicted in Fig. 3. The setup includes a shaft supported by four bearings

powered by an electric motor using a belt. During the experimental lifespan, the shaft experienced a constant speed of 2000 rpm and a constant load of 26.7 kN. 984 one-second-long raw vibration data signals were recorded and made available over the experimental lifespan. The vibration data was recorded at a sampling rate of 20480 Hz [87]. The fault condition that manifested during the experimental lifespan is an outer race bearing fault. The ball pass frequency for the outer race (BPFO), i.e., the frequency of an outer race bearing fault condition [15], for the selected IMS dataset is 236 Hz. This frequency is highlighted as the outer race bearing failure is known a priori [88]. Figure 3(b) visualizes the raw vibration signals' root mean square (RMS) and kurtosis for the considered IMS dataset.

B. BEARING STUDY: LVM SPECIFICATIONS

The LVMs trained on the available 984 raw vibration signals used the Hankelization-based pre-processing step given in Equation (10) with a window length of $L_w = 256$ and a shift of $L_{sft} = 1$. In our initial investigations, we found that an increased window length gave minimal performance improvements for the PPCA and PPCA$_h$ models, while a larger window length impacted the performance of the interpretation-focused model. We believe this is related to the issue identified by Antoni [51] for kurtosis-based methods.

For the PPCA and PPCA$_h$ models, the cumulative contribution rate (CCR)

$$\text{CCR} = \frac{\sum_{j=1}^{d} \lambda_j}{\sum_{j=1}^{D} \lambda_j}, \tag{20}$$

is used to define the size of the latent space d_h and d_i, respectively. The CCR defined in Equation (20) represents the fraction of preserved data variance relative to the total data variance [57]. The CCR for the PPCA model was set to CCR = 80%, while the dimensionality of the SRICA model was set to $d = 20$. The first 10% of the available data was used to train the PPCA$_h$ model with a CCR of 80%.

To validate the choice of latent dimensionality for the SRICA model, the excess kurtosis of the latent components for signals at 25%, 50%, and 75% of the experimental lifespan is investigated for a latent dimensionality range of $d = 2$ to $d = 128$ in increments of $d = 2^j$, where $j = 1, \cdots, 7$. Figure 4 presents the latent excess kurtosis for the considered latent dimensionality range. The latent component kurtosis at 25% and 50% of the experimental lifespan contains little non-Gaussian information of significant interest. However, at 75% of the experimental lifespan, there are prominent components of interest, with a noticeable elbow in the latent kurtosis around $d = 4$. Hence, a latent dimensionality larger than $d = 4$ is sufficient to allow the SRICA model to capture interesting components of the raw vibration data in the online training setting.

C. BEARING STUDY: PERFORMANCE METRICS

To compare the performance of the considered LVMs, two diagnostic metrics are computed using the constructed HI and LHI signals. These metrics provide insight into the fault diagnostic capacity of the considered LVMs and assess their ability to extract diagnostic information from the vibration data. These metrics compare the ability of the extracted temporal-preserving HIs and LHIs for fault detection and localization and demonstrate their ability to perform fault trending.

The RMS of the $HI^{(1)}$ and $LHI^{(1-5)}_{PI|PD}$ signals is computed as the first diagnostic metric to compare offline and online LVMs in the offline and online training settings. The signal-to-noise ratio (SNR) of the square envelope spectrum (SES) is used as a second diagnostic metric to quantify the considered indicators' sensitivity to the bearing fault present. The square envelope (SE) of a signal $x[n]$ is given by

$$\text{SE}[n] = |x[n] + j \cdot H(x[n])|^2, \tag{21}$$

where $j = \sqrt{-1}$ represents the imaginary unit and $H(\cdot)$ represents the Hilbert transform [89]. The SES is given by

$$\text{SES}[k] = |DFT\{\text{SE}[n]\}| \tag{22}$$

where k represents the cyclic frequency and DFT$\{\cdot\}$ is the discrete Fourier transform (DFT). Schmidt *et al.* [73] propose a targeted methodology to determine the SNR based on the SES

$$\text{SNR}_{\text{SES}} = \sum_{h=1}^{N_h} \frac{\max\{\text{SES}[k]\}_{k \in \mathcal{A}_h}}{\text{median}\{\text{SES}[k]\}_{k \in \mathcal{B}_h}}, \tag{23}$$

which represents the prominence of specific spectral components and integer harmonics against the noise floor in the

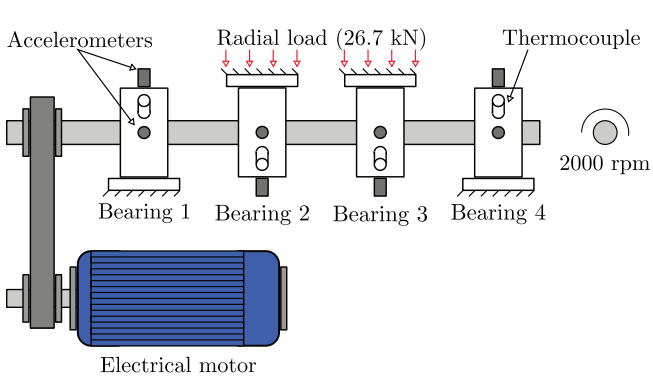

(a) Experimental setup schematic.

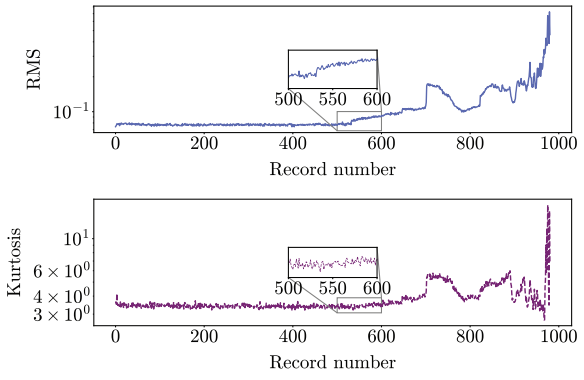

(b) Statistical properties.

Fig. 3. A schematic of the IMS experimental setup and the statistical properties of the raw vibration signals. The statistical properties of the raw vibration signals in (b) are log-scaled for visualization purposes. Please note that these figures are best viewed in color.

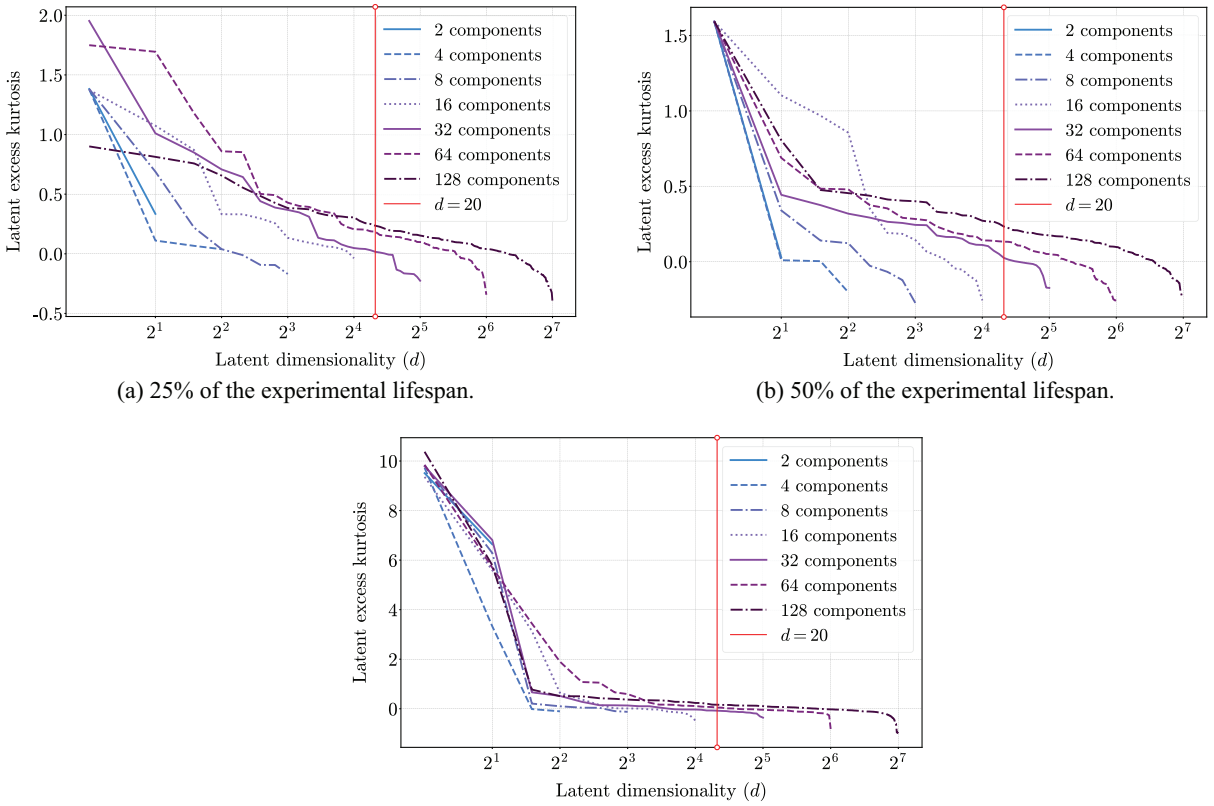

(a) 25% of the experimental lifespan.

(b) 50% of the experimental lifespan.

(c) 75% of the experimental lifespan.

Fig. 4. The latent excess kurtosis for the SRICA models trained at different states of the IMS dataset lifespan. The x-axis of (a), (b), and (c) are $\log_2$ scaled to aid with visualization. Please note that these figures are best viewed in color.

SES within specific cyclic frequency bands. The median of the SES estimates the noise floor within a specific frequency band. The set $\mathcal{A}_h$ represents the indices associated with the h^{th} harmonic of the cyclic frequency α_c of interest within a tolerance range

$$\mathcal{A}_h = \{k | k \in N,\ \alpha_c \cdot (h - \tau_{\mathcal{A}}) \leq \alpha_k \leq \alpha_c \cdot (h + \tau_{\mathcal{A}})\}, \tag{24}$$

where $\tau_{\mathcal{A}}, 0 \leq \tau_{\mathcal{A}} \leq 1$, represents a cyclic frequency tolerance control parameter [33]. The set $\mathcal{B}_{\hbar}$

$$\mathcal{B}_{\hbar} = \{k | k \in N,\ \alpha_c \cdot (h - \tau_{\mathcal{B}}) \leq \alpha_k \leq \alpha_c \cdot (h + \tau_{\mathcal{B}})\}, \tag{25}$$

represents the indices of the frequency band with a bandwidth centered around the h^{th} harmonic of α_c where $\tau_{\mathcal{B}}$ represents the bandwidth parameter, where $0 \leq \tau_{\mathcal{A}} < \tau_{\mathcal{B}} \leq 1$, that captures the SES components between the integer harmonics of the cyclic frequency. Figure 5. visually demonstrates the SNR calculation based on the SES. For this investigation, the first three integer harmonics, i.e., $N_h = 3$, are used as targeted features to compute the SNR_{SES}.

The diagnostic metrics considered in this work are dimensionalized, so we non-dimensionalize them by standardizing them using the first 10% of the available experimental data [91,92]. This ensures that the responsiveness of the considered indicators can be critically compared without scale bias.

A condition deviance (CD) point is identified for the considered diagnostic metrics using a condition interval (CI) calculated using

$$CI = \mu_m \pm 3 \cdot \sigma, \tag{26}$$

where the thresholds' median μ_m and the standard deviation σ are estimated using a percentage of the diagnostic metric values related to the asset in a healthy condition. An abnormal CD point outside the condition interval is identified when the average of five consecutive metrics exceeds the CI bounds. The purpose of the CD points is to enable the identification of health state deviation from a prescribed reference condition. In doing so, a judgment can be made on the ability of the indicators from the considered LVMs to characterize changes in the asset health state and assess their sensitivity to damage. This sensitivity is coupled with the choice of HI and LHI [47].

D. BEARING STUDY: EXPERIMENTAL RESULTS

This section presents the results of the bearing fault investigation. The results are organized as follows: Section III.D.1 displays the outcomes for the first diagnostic metric, Section III.D.2 shows the results for the second diagnostic metric, and Section III.E provides a comparative result analysis and discusses the implications of the considered LVMs.

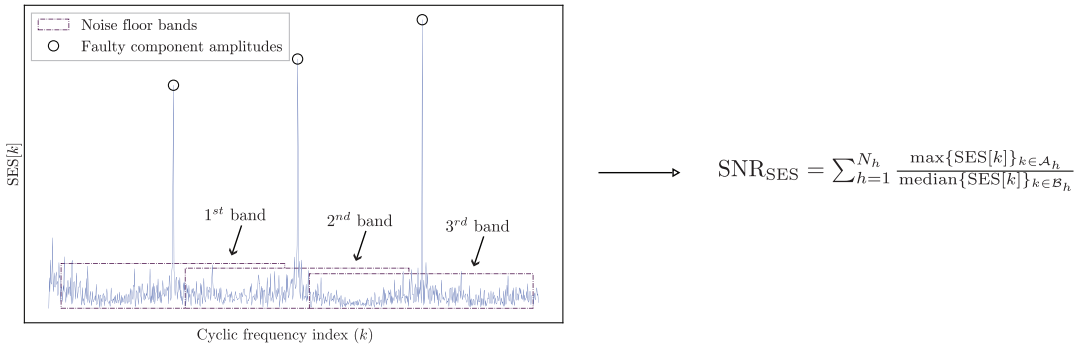

Fig. 5. The procedure to calculate the SNR using the SES for a cyclic component set size is $N_h = 3$ [90].

1. DIAGNOSTIC METRIC ONE: RMS. Figure 6 presents the standardized $\log_{10}(\text{RMS})$ of the condition indicators for the considered offline and online LVMs. Indicator standardization was performed using an estimate of the indicator mean and variance from the first 10% of the available indicator signals. The indicators from the PPCA model, as presented in Fig. 6(a) and Fig. 6(b), exhibit clear sensitivity to the bearing damage present in the considered IMS dataset. Both the PI and PD settings provide fault-sensitive indicators for the PPCA model. Using the identified CD points, the PPCA model is responsive to the onset of damage around record 533, and the $LHI_{PD}^{(3)}$ metric, the normalized Canberra distance, is the least sensitive to the onset of damage. The reconstruction error, $HI^{(1)}$, exhibits the strongest sensitivity for the PPCA model, which indicates that residual fault information is present in the reconstructed data space. It is also evident that the considered latent indicators undergo strong fluctuations from the baseline condition towards the end of the experimental lifespan.

Figure 6(c) and Fig. 6(d) present the results from the SRICA model. Compared to the PPCA model results, the indicators from the SRICA model have less sensitivity in the RMS of the condition indicator signals, except for the $HI^{(1)}$ metric. The PI setting for the SRICA model produces indicators that exhibit better sensitivity to the bearing damage present in the IMS dataset than the PD indicators. In comparing the CD points from the PPCA model to those from the SRICA model, it is evident that the PPCA PI indicators have better sensitivity to the onset of bearing damage present in the data when using the RMS as a diagnostic metric. As with the PPCA model, the $HI^{(1)}$ metric from the SRICA model exhibits stronger sensitivity in the RMS of the condition indicator signal. The PD setting for the SRICA model is noticeably insensitive to the onset and progression of damage, whereby the CD points are located around the strong change in condition present around record 700 (as observed in Fig. 3(b)) is detectable. This suggests that the latent scaling procedure proposed in Equation (13) is less optimal for the IMS dataset.

The RMS of the PPCA_h indicator signals, as presented in Fig. 6(e) and Fig. 6(f), all exhibit sensitivity to the onset of bearing damage except for the $HI^{(1)}$ metric, the reconstruction error, which shows weakened sensitivity and poorer CD identification. The $LHI_{PD}^{(3)}$ and $LHI_{PD}^{(5)}$ metrics from the PPCA_h model, the normalized Canberra distance and the Cosine distance, exhibit more significant fluctuations once the fault occurs, indicating that the latent manifold response to damage captured by these metrics is more complex and this causes a drop below the baseline RMS metric range. In a comparative analysis of the offline and online reconstruction-focused LVMs under consideration, both the PPCA model and the PPCA_h model exhibit the ability to provide distinct RMS deviations to the onset of the localized bearing damage. However, the sensitive indicators are not consistent between the two methods, e.g., $HI^{(1)}$ and $LHI_{PI}^{(2)}$ (the reconstruction error and the normalized Manhattan distance, respectively) in the PI setting and $LHI_{PD}^{(3)}$ and $LHI_{PD}^{(5)}$ (the normalized Canberra distance and the normalized Cosine distance) in the PD setting. This emphasizes the need to use multiple indicators as the best indicators are not known a priori. This is supported by the results from the SRICA model, which exhibits better sensitivity to the onset of damage from the PI indicators than the PD indicators. This emphasizes the need to consider the PI and PD traversal settings when computing LHIs.

The models trained using the online training approach perform well compared to the PPCA_h model trained on reference data. Hence, it is necessary to quantify further the implications of the LVM training procedure and LVM formulation used to determine the sensitivity to the bearing fault present in the data.

2. DIAGNOSTIC METRIC TWO: SNR. In Fig. 7, the indicator's standardized $\log_{10}(\text{SNR})$ value is visualized for the considered offline and online LVMs. The SNR sensitivity investigation is necessary to motivate and quantify the fault isolation characteristics of the considered HI and LHI condition indicators. The condition indicators from the SRICA model, presented in Fig. 7(c) and Fig. 7(d), exhibit clear sensitivity to the IMS outer race bearing fault. The indicators from the PI setting are more sensitive than those from the PD setting and have less noise. However, the indicators from the PPCA model presented in Fig. 7(a) and Fig. 7(b), exhibit weak sensitivity. This difference is also discernible via the identified CD points; the PPCA model only provides CD detection after record 600. Figure 7(e) and Fig. 7(f) indicate that the PPCA_h model has improved sensitivity to the fault present in the data over the PPCA model. Still, the PI indicators from the SRICA model exhibit the best sensitivity overall. For the PPCA_h model, only the $LHI_{PI|PD}^{(4)}$ metrics, the normalized Chebyshev distance, can identify a CD point before the 600^{th} record. This contrasts the results observed in the RMS of the condition indicators presented in Fig. 6, thereby highlighting the implication of the characteristics of the considered offline and online LVMs and the choice of diagnostic metric.

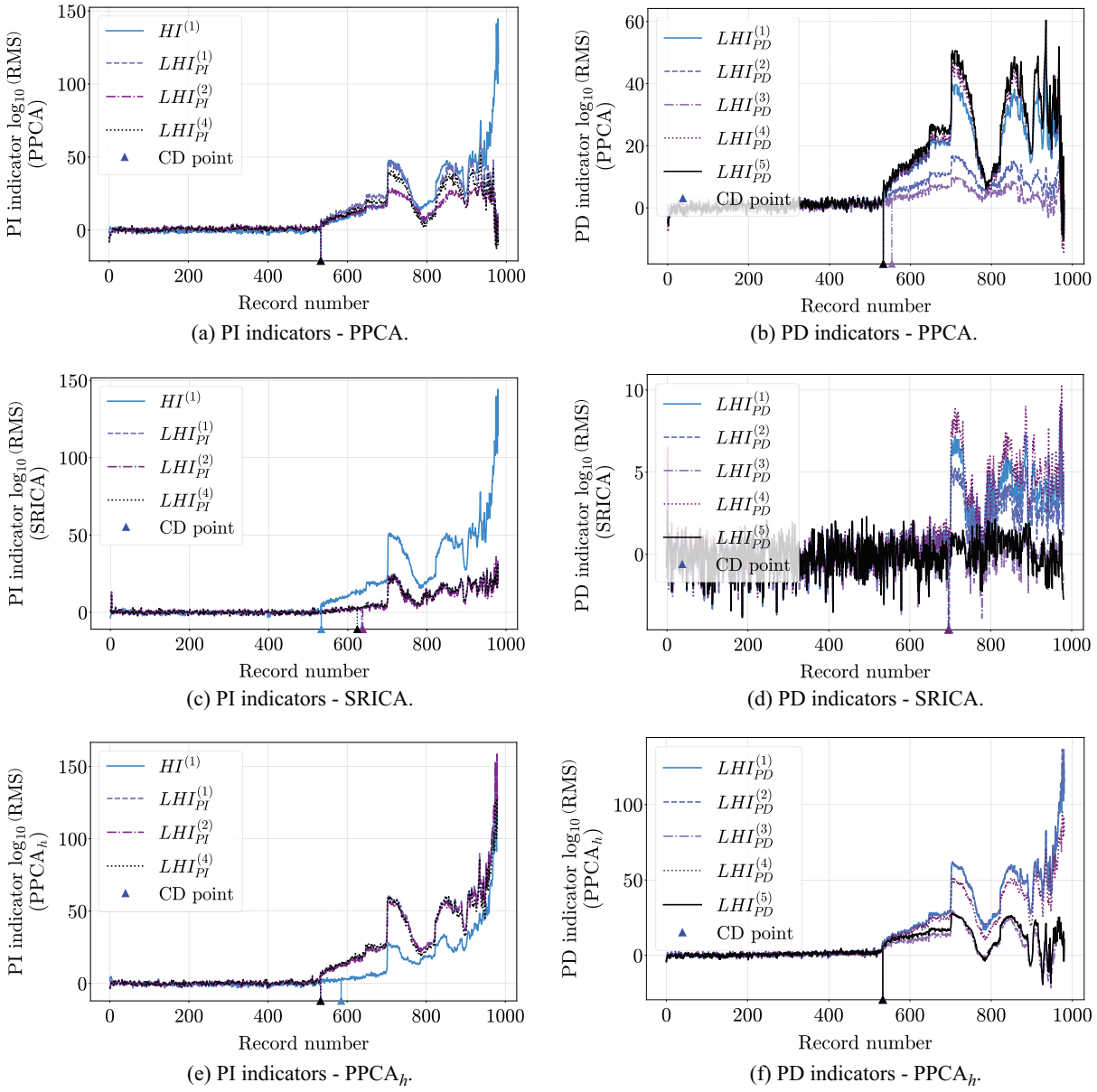

(a) PI indicators - PPCA. (b) PD indicators - PPCA.

(c) PI indicators - SRICA. (d) PD indicators - SRICA.

(e) PI indicators - PPCA$_h$. (f) PD indicators - PPCA$_h$.

Fig. 6. The standardized $\log_{10}(\text{RMS})$ of the indicators for the offline and online LVMs applied to the IMS dataset. The indicators are grouped by LVM formulation and path traversal setting for comparison purposes and log-scaled before standardization for visualization purposes. PI refers to path-independent LHIs, while PD refers to path-dependent LHIs. Please refer to Section II.E for more information. Please note that these figures are best viewed in color

Figure 7(c) indicates that the LHIs from the SRICA model in the PI setting all contain information directly related to the fault of interest. The CD points all identify the change in condition around record 533. In the PD setting, as seen in Fig. 7(d), only the $LHI_{PD}^{(3)}$ indicator, the normalized Canberra distance, from the SRICA model is insensitive to the fault condition present in the data and no CD point is obtained for this indicator. However, the SNR diagnostic metric for the LHIs from the SRICA model in the PD setting has more noise, indicating that the PI setting is better suited to CM tasks for the IMS dataset using this LVM formulation. For the PPCA model SNR results, seen in Fig. 7(a) and Fig. 7(b), the HI and LHI indicators exhibit clear insensitivity to the change in condition around record 533 and only show a noticeable CD detection around record 700.

For the PPCA$_h$ model, CD point identification occurs earlier than record 700, indicating that although the model has strong indicator deviations in its RMS, the bearing fault frequency is less pronounced. Hence, the SRICA model is observed to be the most sensitive to the bearing damage on the IMS dataset, and the characteristics of the LVM better isolate the fault component of interest within the latent manifold. The PPCA and PPCA$_h$ models, in comparison, fail to accurately represent the fault component of interest in the LHIs. This indicates that maximal variance is a useful tool for detecting deviations due to the presence of a fault, but it may only sometimes be useful for inferring the underlying fault condition. This indicates the importance of online interpretation-focused methods, as they may provide an

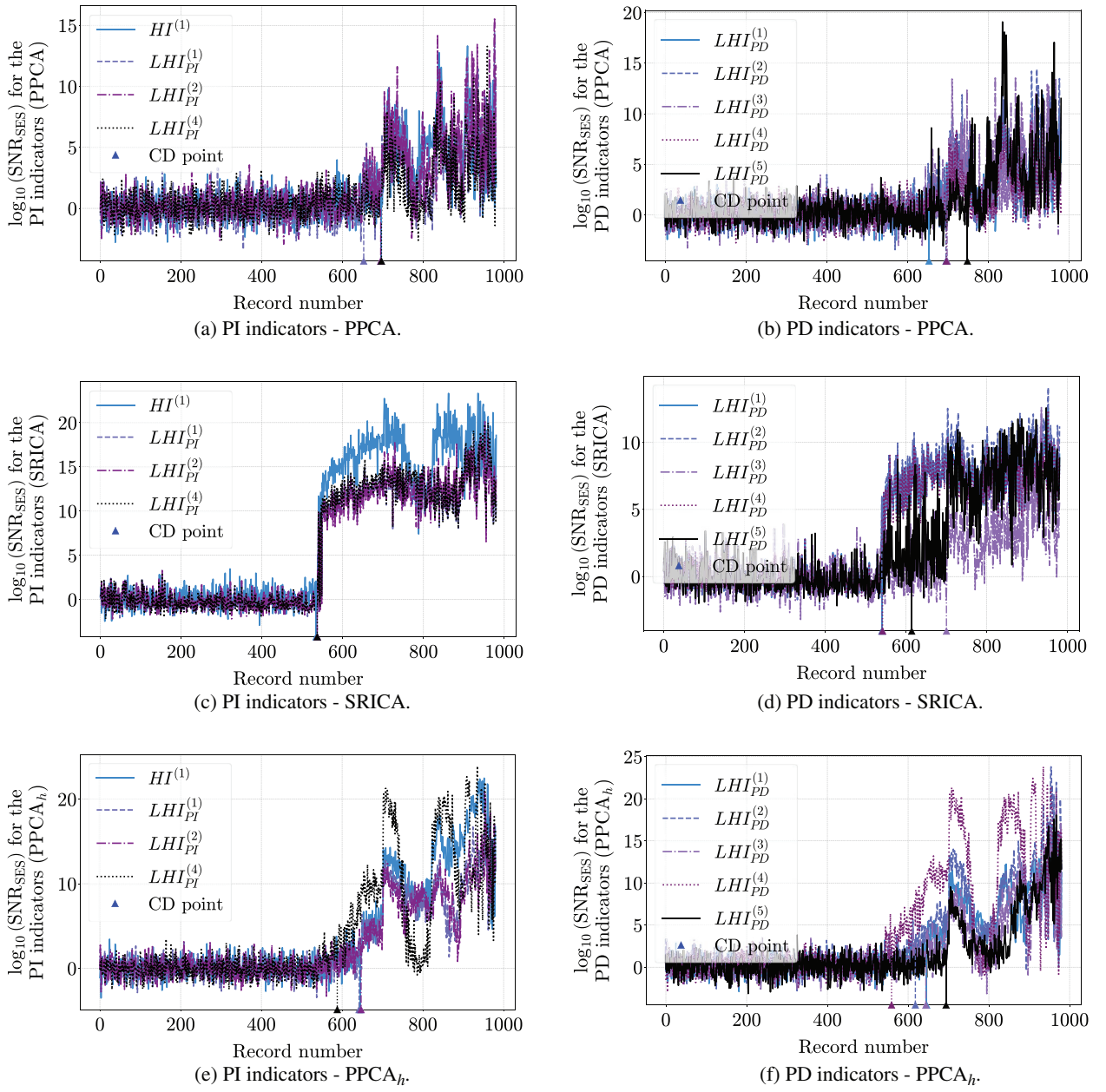

(a) PI indicators - PPCA.
(b) PD indicators - PPCA.
(c) PI indicators - SRICA.
(d) PD indicators - SRICA.
(e) PI indicators - PPCA_h.
(f) PD indicators - PPCA_h.

Fig. 7. The standardized $\log_{10}(\mathrm{SNR})$ was determined using Equation (23) of the indicator signal SES for the considered offline and online LVMs applied to the IMS dataset. The indicators are grouped by LVM formulation and path traversal setting for comparison. The $\mathrm{SNR_{SES}}$ metric is determined using Equation (23). The results are log-scaled before standardization for visualization purposes. Please note that these figures are best viewed in color.

increased capacity to identify the fault signature present in the vibration data.

E. BEARING STUDY: LVM COMPARISON

The results observed in Fig. 6 and Fig. 7 now provide evidence of the complementarity of the reconstruction-focused and interpretation-focused LVMs in the online training setting. The PPCA model responded to the change in the variance of the raw vibration signals over record number but cannot strongly isolate the faulty components of interest in the considered indicators. The SRICA model, in comparison, has weaker sensitivity in the RMS of the considered indicator signals but effectively captures and isolates the bearing fault of interest in the considered PI and PD indicators. This implies that the interpretation-focused LVM is better suited to capture the fault condition present in the IMS dataset. At the same time, the reconstruction-focused LVM is better suited to detecting the change in the variance of the raw vibration signals due to the fault.

Additionally, a comparison of the metrics from the PPCA_h model developed using a reference dataset highlights the implications of the training scheme coupled with the model formulation. Together, the presented findings confirm that the online training setting emphasizes important considerations surrounding the choice of formulation for LVM-based fault diagnostics, and the comparison to the PPCA_h model highlights that the online training approach is a useful LVM setting in CM applications.

IV. EXPERIMENTAL GEARBOX DATASET STUDY

The second considered dataset is an experimental gear fault dataset, characterized by time-varying operating conditions. For this investigation, the key performance metrics are the capacity of the considered offline and online LVMs to detect damage, identify the faulty component of interest, and detect and trend the damage. i.e., to perform fault diagnosis [6,86]. In Section IV.A, an overview of the experimental setup is provided. Section IV.B details the specifications of the considered LVMs, after that Section IV.C presents the selected diagnostic metrics. The results of the second experimental investigation are presented in Section IV.D.

A. GEARBOX STUDY: EXPERIMENTAL SETUP

The Center for Asset Integrity Management (C-AIM) laboratory at the University of Pretoria, South Africa, made the second experimental dataset available. The raw vibration signals used in this section were obtained from the experimental helical gearbox setup detailed in Fig. 8. The setup includes an alternator, three helical gearboxes, and an electrical motor. A total of 300 vibration signals were recorded from a tri-axial accelerometer located behind the center gearbox. Additionally, an optical probe and a zebra tape shaft encoder with 88 angular increments were used to record information related to the input shaft speed. The vibration signals were recorded for 20 seconds at a sampling rate of 25.6 kHz, while the optical probe recorded data at a sampling rate of 51.2 kHz. The first 100 measurements represent the gearbox in a healthy condition, after which a gear tooth was manually seeded with damage, and the setup was run for approximately 20 days until a gear tooth failure occurred. The final 200 measurements were obtained after the artificial fault was seeded, representing the gearbox in an unhealthy condition. The gear of interest at the point of fault introduction and after the experiments were concluded is shown in Fig. 9.

The time-varying operating condition experienced during the experimental lifespan is visualized in Fig. 10(a). Time-varying operating conditions impede the CM task as the instantaneous health state of the gearbox is intertwined with information unrelated to the gear's health state. The raw vibration data also contains prominent impulsive information for all recorded data, regardless of the gear health state. This is attributed to unseen contact between the gearbox casing and a floating bearing when axial shaft loadings were applied to the shaft. The statistical properties of the raw vibration signals are visualized in Fig. 10(b). The impulsive components not corresponding to the gear tooth fault further impede the CM task as prominent diagnostic information is present but unrelated to the component of interest.

B. GEARBOX STUDY: LVM SPECIFICATIONS

The LVMs trained on the 300 raw vibration signals used a window length of $L_w = 512$ and a shift of $L_{sft} = 1$. In our initial investigations, we found that the selected window length improved performance for all the considered LVMs

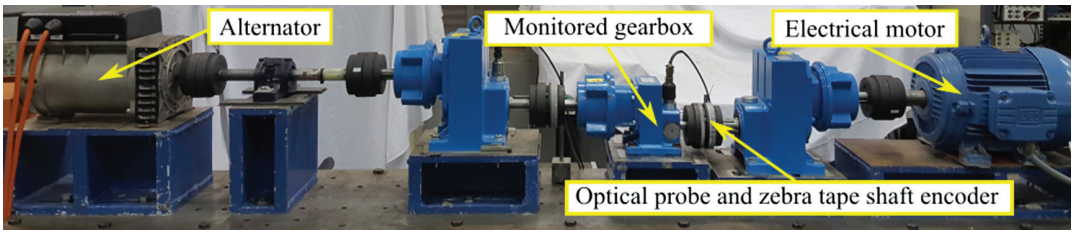

Fig. 8. The experimental gearbox dataset setup.

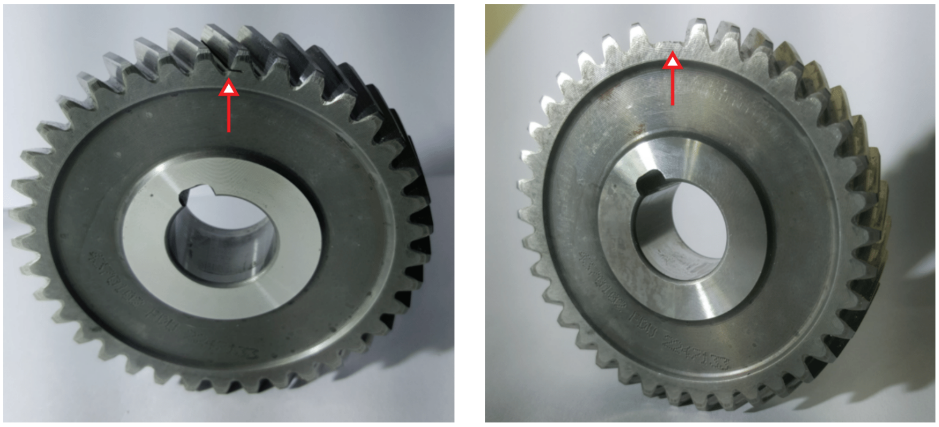

(a) Gear condition – before. (b) Gear condition - after.

Fig. 9. The helical gear used to introduce localized gear tooth damage for the C-AIM gearbox dataset. (a) details the seeded gear tooth failure before experiments were conducted for a damaged gearbox state, and (b) details the helical gear after experiments were concluded.

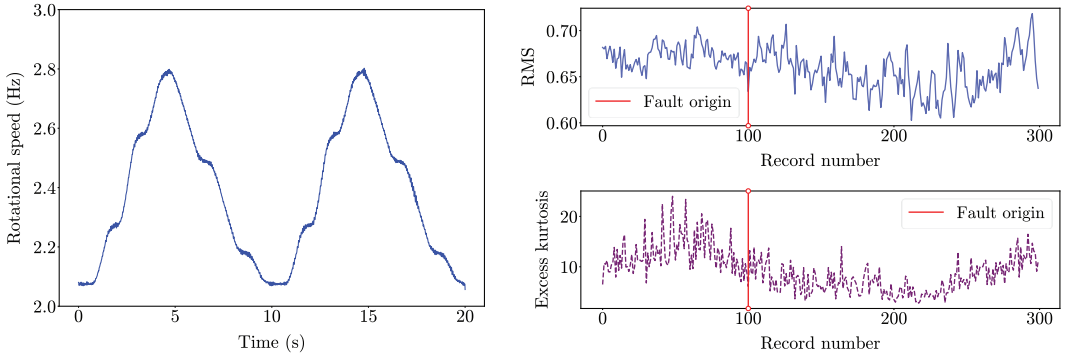

(a) Input shaft operating conditions. (b) Dataset statistical properties.

Fig. 10. The operating conditions experienced by the input gear shaft and the statistical properties of the raw vibration data for the gearbox dataset. It is evident from (b) that the operating conditions and the bearing-related impulsivity impede the condition inference task. The excess kurtosis of the raw vibration data is strongly non-Gaussian, as seen in (b) throughout the experimental lifespan and is highly leptokurtic. The fault origin point in (b) represents the separation between the measurements acquired from the healthy gearbox and the measurements acquired from the gearbox with seeded damage. Please note that these figures are best viewed in color.

when applied to the raw gearbox vibration data. The CCR for the PPCA model was set to CCR = 95%, while the latent dimensionality of the SRICA model was set to $d = 60$. We found that increasing the CCR significantly improved the performance of the PPCA model for the experimental gearbox dataset. However, increasing the CCR for the IMS dataset investigation did not yield a positive performance improvement. This suggests that the CCR is a sensitive parameter important to the performance of reconstruction-focused LVMs for the fault diagnosis task. The first 10% of the available data was used to train the PPCA_h model with a CCR of 95%. To validate the choice of latent dimensionality for the SRICA model, the process described in Section III was used, and the latent dimensionality was increased until $d = 256$. Figure 11 contains the visualization of the kurtosis in this regard. The latent source kurtosis approaches an elbow point around $d = 32$. Hence, the selected latent dimensionality for the SRICA model is suitable for capturing the non-Gaussian components in the raw vibration data.

C. GEARBOX STUDY: PERFORMANCE METRICS

Following the investigation performed in Section III, two diagnostic metrics, computed for HI and LHI signals, are used to compare the performance of the considered LVMs in a fault diagnosis setting.

The synchronous median of the square envelope (SMSE) [93] is used for the gearbox dataset investigation to compare the considered offline and online LVMs. The SMSE is not a diagnostic metric, but a post-processing procedure to heighten the fault condition of interest in the computed HI and LHIs signals. This is possible as a gear tooth fault is assumed a priori for the second dataset. The SMSE of the j^{th} order tracked condition indicator signal from the i^{th} record is given by

$$\text{SMSE}_{\text{j}}(\phi,\Phi_k) = \text{median}(\text{SE}_{\text{j}}(\phi,\Phi_k)) \tag{27}$$

where $\text{median}(\cdot)$ represents the median statistic, $\phi \in [0,\Phi_k)$ refers to the angular position, Φ_k refers to the cyclic period, and $\text{SE}_{\text{j}}(\phi,\Phi_k)$ is the order tracked SE of the j^{th} condition indicator signal. As the condition indicator signals are order tracked, deviations related to the gear tooth fault are expected to be synchronous with the gear shaft rotation, i.e., $\Phi_k = 2\pi$. The SMSE is an extension of the SE (SASE) synchronous average and is more robust in the presence of impulsive non-synchronous components [93]. Hence, it is well suited for the investigation of the gearbox dataset.

As the gear fault is known a priori, the objective is to ascertain the sensitivity of the condition indicators from the considered offline and online LVMs to this fault. Two diagnostic metrics are used to conduct such an investigation. First, the RMS of the region within the SMSE corresponding to the gear tooth fault is used. Second, the SNR of the SMSE signals is determined via

$$\text{SNR}^{\text{dB}}_{\text{SMSE}} = 20\log\left(\frac{A^{\text{SMSE}}_{j,\text{damaged}}}{A^{\text{SMSE}}_{j,\text{healthy}}}\right), \tag{28}$$

where $A^{\text{SMSE}}_{j,\text{damaged}}$ and $A^{\text{SMSE}}_{j,\text{healthy}}$ represent the RMS of the damaged portion and the healthy portion of the j^{th} SMSE signal is evaluated using the logarithmic decibel (dB) scale. The $\text{SNR}^{\text{dB}}_{\text{SMSE}}$ metric is used to quantify how prominent the fault component of interest is against the noise floor. Figure 12 demonstrates the SMSE condition quantification methodology used in this work for the experimental gearbox dataset.

D. GEARBOX STUDY: EXPERIMENTAL RESULTS

This section reports the findings of the experimental gear fault investigation, with the results structured as follows: Section IV.D.1 presents the results for the first diagnostic metric, followed by the results from the second diagnostic metric in Section IV.D.2. Finally, Section IV.E compares and discusses the implications of the considered LVMs based on the learnings from the results observed in Section IV.D.1 and Section IV.D.2. Following the approach used in Section III.D, the diagnostic metrics are standardized, and a CD point is identified for each of the HIs and LHIs to ensure that the indicators can be effectively compared and investigated.

1. DIAGNOSTIC METRIC ONE: RMS. Figure 13 presents the standardized RMS of the SMSE metric for the indicators

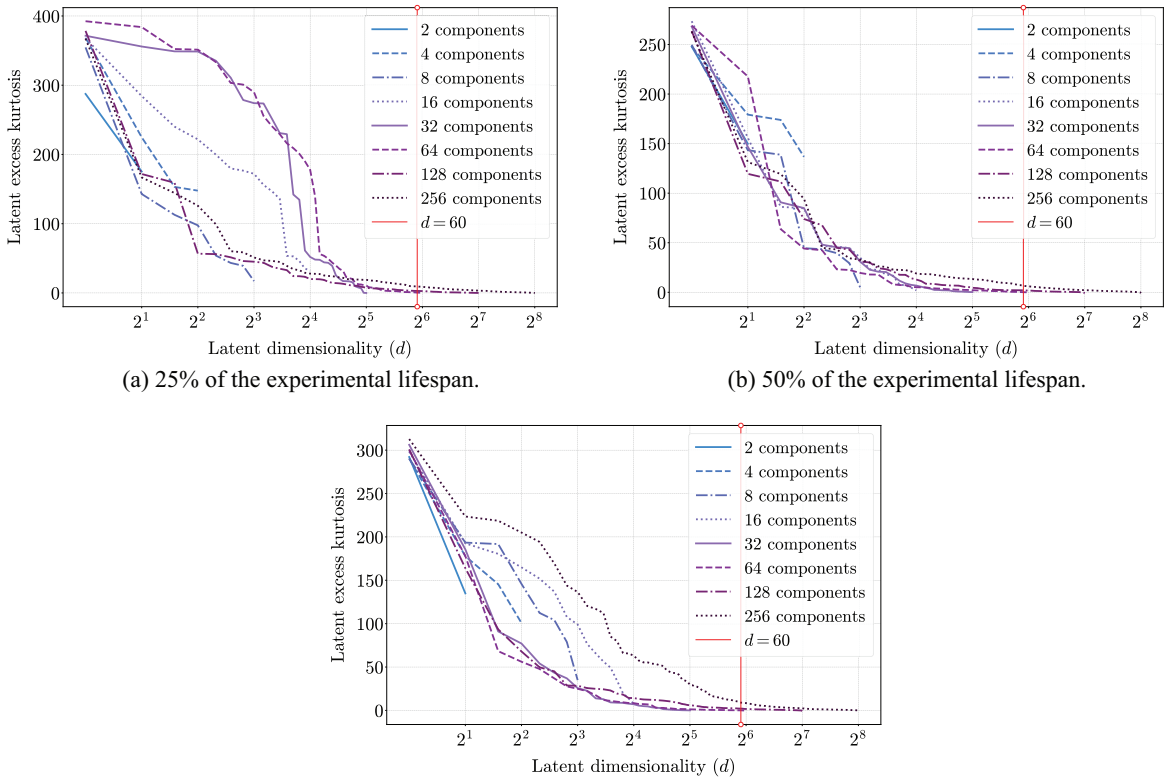

(a) 25% of the experimental lifespan.

(b) 50% of the experimental lifespan.

(c) 75% of the experimental lifespan.

Fig. 11. The latent excess kurtosis for the SRICA models trained at different states of the experimental gearbox lifespan. The x-axis of (a), (b), and (c) are $\log_2$ scaled to aid with visualization. Please note that these figures are best viewed in color.

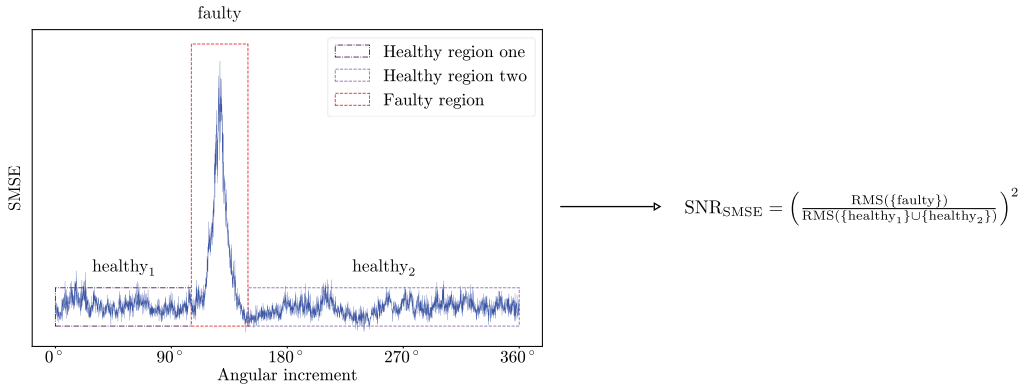

Fig. 12. The procedure used to calculate the SNR of the SMSE signals for the gearbox dataset. The union of sets $\{\text{healthy}_1\}$ and $\{\text{healthy}_2\}$ represent the noise floor of the SMSE, while the set $\{\text{faulty}\}$ represents the damaged portion of the SMSE.

used in this work. The PI indicators from the PPCA model and the SRICA model, presented in Fig. 13(a) and Fig. 13(c), both exhibit a clear variation in condition from the manual fault origin point introduced at record 100. However, the $HI^{(1)}$ metric, the reconstruction error from the PPCA model erroneously identifies a CD point before record 100, which indicates that the PPCA model has some sensitivity to the non-stationarity in the data. The $HI^{(1)}$ metric from the SRICA model exhibits weaker sensitivity to the localized tooth damage, indicating that the latent manifold is more sensitive to the fault condition present in the data. The PD indicators from the PPCA model and the SRICA model, presented in Fig. 13(b) and Fig. 13(d), respectively, exhibit an increased sensitivity to the non-stationarity in the data and less sensitivity to the onset of gear tooth damage. For the PD indicators from the PPCA model, this non-stationarity sensitivity is more pronounced as CD points are identified before record 100. Additionally, the $LHI^{(3)}_{PD}$ metric, the normalized Canberra distance, undergoes a decrease in value around record 100, indicating that this metric decreases in magnitude around the tooth fault location. As both LVMs developed using the online training approach are responsive to the onset of gear tooth damage, it can be concluded that the manifestation mechanism for the gear tooth damage is both variance-driven and non-Gaussian in nature.

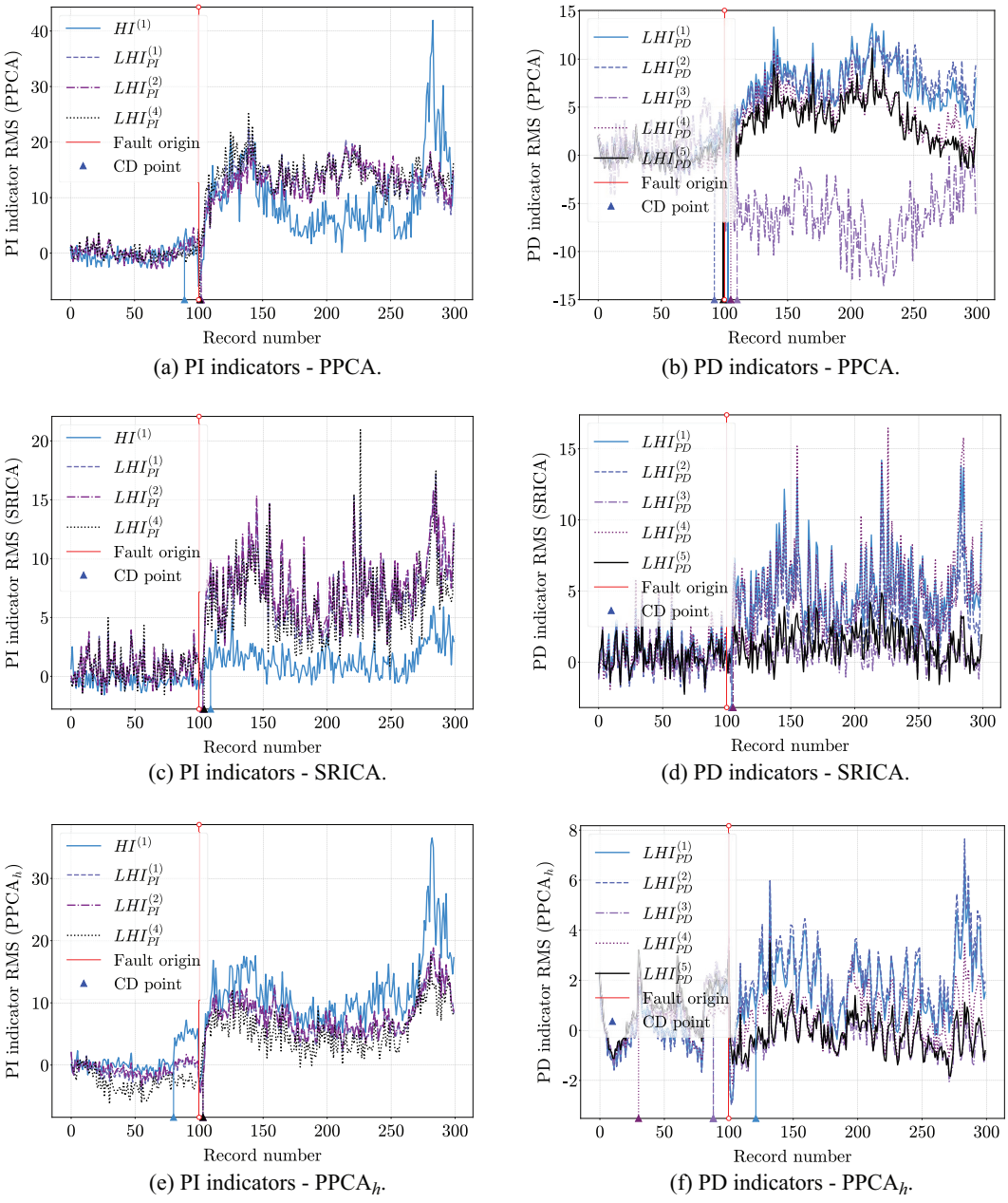

(a) PI indicators - PPCA.
(b) PD indicators - PPCA.
(c) PI indicators - SRICA.
(d) PD indicators - SRICA.
(e) PI indicators - PPCA$_h$.
(f) PD indicators - PPCA$_h$.

Fig. 13. The standardized RMS of the SMSE for the indicators from the considered offline and online LVMs applied to the gearbox dataset. The indicators are grouped by LVM formulation and path traversal setting for comparison. In (a)–(f), the fault origin point is indicated to mark when damage is present in the raw vibration data, enhancing the interpretability of the indicator metrics and their corresponding CD points. This annotation enables a clearer understanding of the relationship between the considered indicators and the onset of damage. Please note that these figures are best viewed in color.

Hence, both considered online LVMs can effectively capture the variation in asset condition. This highlights the complementarity of the considered online LVMs in a fault diagnostic setting and enforces that the LVM formulation is an important consideration for CM using the online training setting. The performance of the PD indicators further highlights the implications of the considered HIs and LHIs used in this work, as damage manifestation locality within the facets of LVMs is not known a priori.

The PPCA$_h$ results presented in Fig. 13(e) and Fig. 13(f) also indicate that the PI setting is better suited to the CM task for the gearbox dataset as it captures less non-stationary information and is more sensitive to the onset of damage. For the PPCA$_h$ model, the CD point of the $HI^{(1)}$ metric occurs before record 100, which indicates a clear sensitivity to the non-stationarity in the healthy gearbox data. The RMS of the PI indicators from the PPCA$_h$ model exhibits clearer sensitivity to the onset of the gear tooth fault. The PD indicators from the PPCA$_h$ model are more sensitive to the data non-stationarity, identified via the erroneously identified CD points and the clear variations in RMS metric value for both the healthy and unhealthy gearbox data.

Hence, the ability to detect and identify an onset of gear tooth damage is affected by the choice of training approach, the LVM formulation used, and the choice of LHI. While the RMS allows for an investigation into the discernability

of the tooth fault, the calculation of the SNR in Equation (28) quantifies tooth damage sensitivity relative to the noise floor, which naturally removes any potential sensitivity to non-stationarity in the data and can better quantify damage detectability performance.

2. DIAGNOSTIC METRIC TWO: SNR. Figure 14 presents the standardized SNR of the SMSE for the indicators used in this work. The identification of the CD points now occurs after record 100, and indicators with worsened sensitivity to the onset of damage can be identified for the offline and online LVMs. As the SNR represents the sensitivity of the tooth fault region in the SMSE with respect to the noise floor, it is possible to further compare the indicator responses from the considered offline and online LVMs. In a comparison of the PI indicators presented in Fig. 14(a), Fig. 14(c), and Fig. 14(e), the PPCA and SRICA models exhibit diagnostic metric responses with similar sensitivity to the gear tooth fault. However, the $HI^{(1)}$ metric from the SRICA model, presented in Fig. 14(c), is less sensitive to the onset of damage than the indicators constructed using the latent manifold. The $LHI^{(4)}_{PD}$ metric, the normalized Chebyshev distance, response from the PPCA$_h$ model, presented in Fig. 14(e), performs worse than the other indicators due to the significant fluctuations in the indicator value attributed to sensitivity to the data non-stationarity.

The PI indicators from the latent manifold of the PPCA and SRICA models, captured in Fig. 14(a) and Fig. 14(c), respectively, have improved sensitivity to the onset of damage over the PI indicators from PPCA$_h$ model, seen

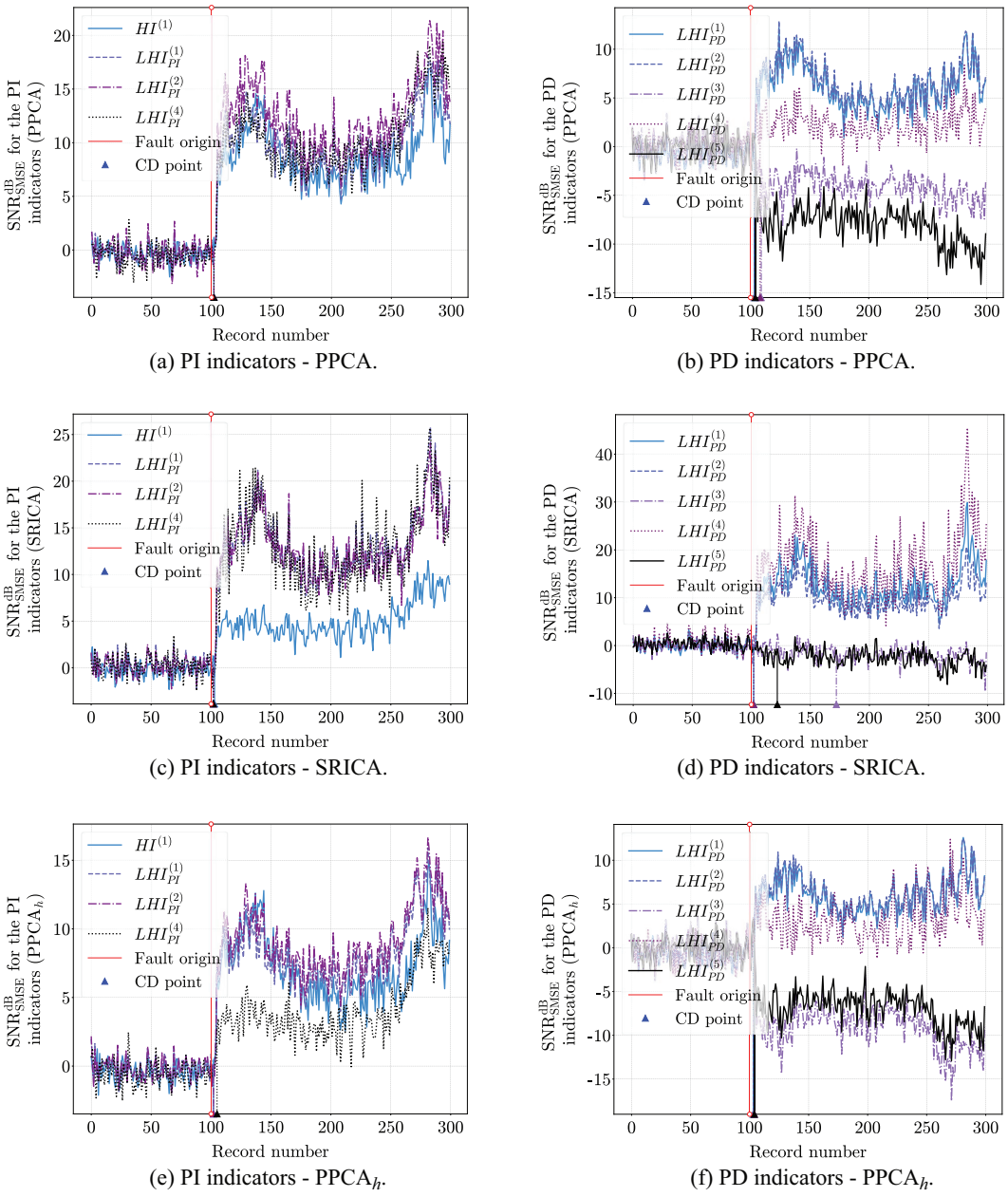

(a) PI indicators - PPCA.
(b) PD indicators - PPCA.
(c) PI indicators - SRICA.
(d) PD indicators - SRICA.
(e) PI indicators - PPCA$_h$.
(f) PD indicators - PPCA$_h$.

Fig. 14. The standardized SNR of the indicator SMSE for the considered offline and online LVMs applied to the gearbox dataset. The SNR is calculated with Equation (28), where Fig. 12 demonstrates the SNR calculation process. The indicators are grouped by LVM formulation and path traversal setting for comparison. Please note that these figures are best viewed in color.

in Fig. 14(e). This indicates that they have enhanced separability between the fault and healthy regions in the SMSE of the HI and LHI signals. This further emphasizes the implications of the LVM formulation and the choice of LVM training setting. In the case of the gearbox dataset, the choice of offline or online training and the LVM formulation used therein appears to have a less significant impact on the early detection of damage onset compared to the IMS dataset. However, there are still noticeable and identifiable implications. Figure 14 indicates that the online training setting is a useful setting for LVMs as there are clear responses to the gear tooth fault, and this is substantiated by comparing the results to those obtained from the PPCA_h model.

E. GEARBOX STUDY: LVM COMPARISON

In a comparison of the PD indicators for the considered offline and online LVMs, presented in Fig. 14(b), Fig. 14(d), and Fig. 14(f), the SNR results indicate that most indicators are sensitive to the change in condition due to the manual fault seeding process, but are in general less sensitive than their PI counterparts. This enforces the implications of the considered LHIs, as each latent manifold extracts unique characteristics from the raw vibration data. Furthermore, the SNR results help quantify the RMS results seen in Fig. 13(b), Fig. 13(d), and Fig. 13(f), whereby the prominence of the faulty component can be inferred relative to the healthy region of the SMSE. By normalizing the RMS results for the PD indicators, thereby removing the inclusion of any per-record non-stationarity, it is possible to quantify the sensitivity of the indicators from the considered offline and online LVMs to the gear tooth fault. Thus, the improvement in the PD indicator captured in the $\text{SNR}^{\text{dB}}_{\text{SMSE}}$ results further highlights that the PD indicators are more sensitive to data's non-stationarity and less sensitive to the onset of the gear tooth damage.

For the PPCA and PPCA_h models, the $LHI^{(3)}_{PD}$ and $LHI^{(5)}_{PD}$ metrics (the Canberra distance and the cosine distance, respectively) have decreasing SNR trends, which indicates that these metrics respond via a reduction in magnitude around the gear tooth fault. This result was only observable for the $LHI^{(3)}_{PD}$ indicator when using the RMS diagnostic metric for the PPCA model, as demonstrated in Fig. 13(b). This indicates that the latent response to the gear tooth fault is to project the anomalous data into regions where the latent representations lie closer together. The same observation can be made for the metrics from the PPCA_h model. This result emphasizes the need for a two-sided threshold when using the indicators. However, the metrics for the SRICA model are insensitive to the onset and progression of the damage. These results further highlight the complementarity of the choice of training framework and LVM framework for CM, whereby the offline and online LVMs exhibit uniqueness in both the indicators sensitive to damage and in the damage manifestation mechanism within the latent manifold.

V. CONCLUSION

This work investigates offline and online training approaches for LVM-based fault diagnostics applied to vibration data. The LVMs considered in this work represent reconstruction-focused and interpretation-focused LVM formulations driven to obtain latent representations that maximize the explained variance and the non-Gaussianity from the observed vibration data. The considered offline and online LVMs extract unique characteristics from the raw data, and the offline and online training approaches were used to ensure that the unique LVM characteristics and implications can be investigated and compared for LVM-based CM applications. A simple set of HIs and LHIs was considered to investigate the sensitivity of the offline and online LVMs as a tool to perform fault diagnostics in different gearbox fault conditions and to study the implication of the online training approach for LVMs.
The results seen in this work demonstrate that:

1. Online reconstruction-focused and interpretation-focused LVMs complement vibration-based condition inference tasks using the online training approach. The choice of online LVM formulation influences the diagnostic information obtained for condition inference. Specifically:
   a. The IMS dataset results indicate that while the reconstruction-focused formulation is sensitive to the change in the data due to damage and useful for early damage detection, the interpretation-focused formulation demonstrates an improved ability to identify and isolate the fault type present in the data.
   b. The gearbox dataset results emphasize that online reconstruction-focused and interpretation-focused LVM formulations possess a complementary capacity to detect the gear tooth damage in the dataset. This highlights the significance of the unique characteristics inherent to the selected LVM formulations and that their suitability to different potential fault conditions is not predetermined.
2. The online training approach used in this work is a useful LVM training setting, and the considered online reconstruction-focused and interpretation-focused LVMs developed using this approach are useful for fault diagnostics. The choice of LVM training framework provides different implications depending on the considered dataset and LVM formulation used.
3. The choice of condition indicator for offline and online LVMs is diverse. Hence, it is important to select metrics that utilize the data space and the latent manifold when applying LVMs. Furthermore, using multiple LHIs for condition inference is beneficial, as the optimal LHI for fault diagnosis purposes is unknown a priori.

The two experimental datasets were used to investigate the sensitivity of offline and online LVMs and the associated HIs and LHIs. The interpretation-focused LVM proved better for isolating the bearing fault in the first dataset. For the second dataset, the offline and online LVMs performed equivalently in a fault diagnosis setting. The results suggest a fault-type dependency when using reconstruction-focused and interpretation-focused online LVMs. However, the optimal choice of formulation for specific fault conditions has yet to be discovered a priori. The diversity in LHI performance across datasets emphasizes the need for multiple LHIs to capture the intricacies of damage manifestation within the latent manifold for accurate condition inference. Hence, as the fault diagnosis task was used to compare offline and online LVMs, it can be concluded that the online training setting is a useful LVM training

approach for reconstruction-focused and interpretation-focused online LVMs in vibration-based fault diagnostics. Furthermore, the choice of training approach and LVM formulation is an important consideration in LVM-based CM applications.

For future work, it is recommended that focus be given to reconstruction-focused and interpretation-focused LVM formulations with nonlinear transition functions. The implications of online training must be further investigated with the nonlinear LVMs as they may provide a more expressive latent manifold, which may benefit the LVM-based CM task. Additionally, the latent scaling approach used in this work for the SRICA model requires further investigation regarding its suitability to vibration-based CM problems. Therefore, alternative scaling strategies should be investigated and considered, or interpretation-focused LVMs, which require no pre-whitening, should be considered. Moreover, alternative LHIs must be investigated for online LVMs to further study the implications of online training. Then, consideration of the full CM problem must occur to assess further the implications of using temporal-preserving LVMs. The automatic selection of the model window length should also be considered in future investigations. Finally, further investigation into complex operating environments must occur to uncover the limits of the considered offline and online LVMs. This will ensure that a suitable level of attention can be given to the complex operating environment problem to develop and improve data-driven methodologies for vibration-based fault diagnostics.

ACKNOWLEDGMENTS

The authors gratefully acknowledge the support received from AngloGold Ashanti in executing this research.

CONFLICT OF INTEREST STATEMENT

The authors declare no conflicts of interest.

REFERENCES

[1] A. K. S. Jardine, D. Lin, and D. Banjevic, "A review on machinery diagnostics and prognostics implementing condition-based maintenance," *Mech Syst Signal Process.,* vol. 20, pp. 1483–1510, 2006.

[2] J. Lee, F. Wu, W. Zhao, M. Ghaffari, L. Liao, and D. Siegel, "Prognostics and health management design for rotary machinery systems—Reviews, methodology and applications," *Mech Syst Signal Process.,* vol. 42, pp. 314–334, 2014.

[3] R. B. Randall, "*Vibration-Based Condition Monitoring: Industrial, Aerospace and Automotive Applications,*" Chichester, UK: Wiley, 2011.

[4] D. Wang, K.-L. Tsui, and Q. Miao, "Prognostics and health management: a review of vibration based bearing and gear health indicators," *IEEE Access,* vol. 6, pp. 665–676, 2018.

[5] A.K.S. Jardine, D. Lin, and D. Banjevic, "A review on machinery diagnostics and prognostics implementing condition-based maintenance," *Mech Syst Signal Process.,* vol. 20, pp. 1483–1510, 2006.

[6] M. Cerrada, R. V. Sánchez, C. Li, F. Pacheco, D. Cabrera, J. Valente de Oliveira, and R. E. Vásquez, "A review on data-driven fault severity assessment in rolling bearings," *Mech Syst Signal Process.,* vol. 99, pp. 169–196, 2018.

[7] R. B. Randall, "*Introduction and background, in: Vibration-Based Condition Monitoring: Industrial, Aerospace and Automotive Applications,*" Chichester, UK: Wiley, 2011.

[8] S. M. Talai, D. A. Desai, and P. S. Heyns, "Comparison of infrared thermography and miniature Deltatron accelerometer sensors in the measurement of structural vibration characteristics," *African Journal of Science, Technology, Innovation and Development.,* vol. 9, pp. 339–348, 2017.

[9] H. Zhao, H. Liu, W. Hu, and X. Yan, "Anomaly detection and fault analysis of wind turbine components based on deep learning network," *Renew Energy.,* vol. 127, pp. 825–834, 2018.

[10] A. Albarbar, F. Gu, and A. D. Ball, "Diesel engine fuel injection monitoring using acoustic measurements and independent component analysis," *Measurement,* vol. 43, pp. 1376–1386, 2010.

[11] O. H. Omoregbee and P. S. Heyns, "Low speed rolling bearing diagnostics using acoustic emission and higher order statistics techniques," *Journal of Mechanical Engineering Research & Developments.,* vol. 41, pp. 18–23, 2018.

[12] J. Zhu, J. M. Yoon, D. He, and E. Bechhoefer, "Online particle-contaminated lubrication oil condition monitoring and remaining useful life prediction for wind turbines," *Wind Energy,* vol. 18, pp. 1131–1149, 2015.

[13] J. P. Salameh, S. Cauet, E. Etien, A. Sakout, and L. Rambault, "Gearbox condition monitoring in wind turbines: a review," *Mech Syst Signal Process.,* vol. 111, pp. 251–264, 2018.

[14] R. Zimroz, W. Bartelmus, T. Barszcz, and J. Urbanek, "Diagnostics of bearings in presence of strong operating conditions non-stationarity—a procedure of load-dependent features processing with application to wind turbine bearings," *Mech Syst Signal Process.,* vol. 46, pp. 16–27, 2014.

[15] R. B. Randall and J. Antoni, "Rolling element bearing diagnostics - a tutorial," *Mech Syst Signal Process.,* vol. 25, pp. 485–520, 2011.

[16] N. Baydar and A. Ball, "A comparative study of acoustic and vibration signals in detection of gear failures using Wigner–Ville distribution," *Mech Syst Signal Process.,* vol. 15, pp. 1091–1107, 2001.

[17] N. Baydar and A. Ball, "Detection of gear failures via vibration and acoustic signals using wavelet transform," *Mech Syst Signal Process.,* vol. 17, pp. 787–804, 2003.

[18] P. Večeř, M. Kreidl, and R. Šmíd, "Condition indicators for gearbox condition monitoring systems," *Acta Polytechnica.,* vol. 45, pp. 35–43, 2005.

[19] J. Lin and M. Zhao, "A review and strategy for the diagnosis of speed-varying machinery," in 2014 *International Conference on Prognostics and Health Management*, IEEE, 2014: pp. 1–9. https://doi.org/10.1109/ICPHM.2014.7036368.

[20] Y. Lei, N. Li, L. Guo, N. Li, T. Yan, and J. Lin, "Machinery health prognostics: a systematic review from data acquisition to RUL prediction," *Mech Syst Signal Process.,* vol. 104, pp. 799–834, 2018.

[21] Y. Lei, B. Yang, X. Jiang, F. Jia, N. Li, and A. K. Nandi, "Applications of machine learning to machine fault diagnosis: a review and roadmap," *Mech Syst Signal Process.,* vol. 138, p. 106587, 2020.

[22] H. Zhou, X. Huang, G. Wen, Z. Lei, S. Dong, P. Zhang, and X. Chen, "Construction of health indicators for condition monitoring of rotating machinery: a review of the research," *Expert Syst Appl.,* vol. 203, p. 117297, 2022.

[23] V. Sharma and A. Parey, "A review of gear fault diagnosis using various condition indicators," *Procedia Eng.,* vol. 144, pp. 253–263, 2016.

[24] N. Baydar and A. D. Ball, "Detection of gear deterioration under varying load conditions by using the instantaneous power spectrum," *Mech Syst Signal Process.,* vol. 14, pp. 907–921, 2000.

[25] C. J. Stander, P. S. Heyns, and W. Schoombie, "Using vibration monitoring for local fault detection on gears operating under fluctuating load conditions," *Mech Syst Signal Process.,* vol. 16, pp. 1005–1024, 2002.

[26] H. Qiu, J. Lee, J. Lin, and G. Yu, "Wavelet filter-based weak signature detection method and its application on rolling element bearing prognostics," *J Sound Vib.,* vol. 289, pp. 1066–1090, 2006.

[27] Y. Lei, J. Lin, Z. He, and M. J. Zuo, "A review on empirical mode decomposition in fault diagnosis of rotating machinery," *Mech Syst Signal Process.,* vol. 35, pp. 108–126, 2013.

[28] J. I. Taylor, "Identification of bearing defects by spectral analysis," *J Mech Des N Y,* vol. 102, pp. 199–204, 1980.

[29] J. Antoni, F. Bonnardot, A. Raad, and M. El Badaoui, "Cyclostationary modelling of rotating machine vibration signals," *Mech Syst Signal Process.,* vol. 18, pp. 1285–1314, 2004.

[30] J. Antoni, "Cyclostationarity by examples," *Mech Syst Signal Process.,* vol. 23, pp. 987–1036, 2009.

[31] P. D. McFadden and J. D. Smith, "Vibration monitoring of rolling element bearings by the high-frequency resonance technique — a review," *Tribol Int.,* vol. 17, pp. 3–10, 1984.

[32] N. Sawalhi, R. B. Randall, and H. Endo, "The enhancement of fault detection and diagnosis in rolling element bearings using minimum entropy deconvolution combined with spectral kurtosis," *Mech Syst Signal Process.,* vol. 21, pp. 2616–2633, 2007.

[33] W. A. Smith, P. Borghesani, Q. Ni, K. Wang, and Z. Peng, "Optimal demodulation-band selection for envelope-based diagnostics: a comparative study of traditional and novel tools," *Mech Syst Signal Process.,* vol. 134, p. 106303, 2019.

[34] Y. Miao, B. Zhang, J. Lin, M. Zhao, H. Liu, Z. Liu, and H. Li, "A review on the application of blind deconvolution in machinery fault diagnosis," *Mech Syst Signal Process.,* vol. 163, p. 108202, 2022.

[35] V. Sinitsin, O. Ibryaeva, V. Sakovskaya, and V. Eremeeva, "Intelligent bearing fault diagnosis method combining mixed input and hybrid CNN-MLP model," *Mech Syst Signal Process.,* vol. 180, p. 109454, 2022.

[36] X. Gu, Y. Yu, L. Guo, H. Gao, and M. Luo, "CSWGAN-GP: A new method for bearing fault diagnosis under imbalanced condition," *Measurement,* vol. 217, p. 113014, 2023.

[37] Z. Zhang, S. Xu, and H. Chen, "Discriminative feature learning and selection with label-induced sparse filtering for intelligent fault diagnosis of rotating machinery," *Mech Syst Signal Process.,* vol. 196, p. 110338, 2023.

[38] R. Wang, F. Yan, L. Yu, C. Shen, X. Hu, and J. Chen, "A federated transfer learning method with low-quality knowledge filtering and dynamic model aggregation for rolling bearing fault diagnosis," *Mech Syst Signal Process.,* vol. 198, p. 110413, 2023.

[39] J. Chen, R. Huang, Z. Chen, W. Mao, and W. Li, "Transfer learning algorithms for bearing remaining useful life prediction: A comprehensive review from an industrial application perspective," *Mech Syst Signal Process.,* vol. 193, p. 110239, 2023.

[40] W. Li, R. Huang, J. Li, Y. Liao, Z. Chen, G. He, R. Yan, and K. C. Gryllias, "A perspective survey on deep transfer learning for fault diagnosis in industrial scenarios: Theories, applications and challenges," *Mech Syst Signal Process.,* vol. 167, p. 108487, 2022.

[41] Q. Qian, Y. Qin, J. Luo, Y. Wang, and F. Wu, "Deep discriminative transfer learning network for cross-machine fault diagnosis," *Mech Syst Signal Process.,* vol. 186, p. 109884, 2023.

[42] W. Booyse, D. N. Wilke, and P. S. Heyns, "Deep digital twins for detection, diagnostics and prognostics," *Mech Syst Signal Process.,* vol. 140, p. 106612, 2020.

[43] R. Balshaw, P. S. Heyns, D. N. Wilke, and S. Schmidt, "Importance of temporal preserving latent analysis for latent variable models in fault diagnostics of rotating machinery," *Mech Syst Signal Process.,* vol. 168, p. 108663, 2022.

[44] K. Huang, S. Wu, B. Sun, C. Yang, and W. Gui, "Metric learning-based fault diagnosis and anomaly detection for industrial data With intraclass variance," *IEEE Trans Neural Netw Learn Syst.,* vol. 35, pp. 547–558, 2024.

[45] O. Fink, Q. Wang, M. Svensén, P. Dersin, W.-J. Lee, and M. Ducoffe, "Potential, challenges and future directions for deep learning in prognostics and health management applications," *Eng Appl Artif Intell.,* vol. 92, pp. 103678, 2020.

[46] J. Lee, F. Wu, W. Zhao, M. Ghaffari, L. Liao, and D. Siegel, "Prognostics and health management design for rotary machinery systems—Reviews, methodology and applications," *Mech Syst Signal Process.,* vol. 42, pp. 314–334, 2014.

[47] R. Balshaw, P. S. Heyns, D. N. Wilke, and S. Schmidt, "Latent indicators for temporal-preserving latent variable models in vibration-based condition monitoring under non-stationary conditions," *Mech Syst Signal Process.,* vol. 199, p. 110446, 2023.

[48] T. Heyns, P. S. Heyns, and J. P. de Villiers, "Combining synchronous averaging with a Gaussian mixture model novelty detection scheme for vibration-based condition monitoring of a gearbox," *Mech Syst Signal Process.,* vol. 32, pp. 200–215, 2012.

[49] S. Schmidt, P. S. Heyns, and J. P. de Villiers, "A novelty detection diagnostic methodology for gearboxes operating under fluctuating operating conditions using probabilistic techniques," *Mech Syst Signal Process.,* vol. 100, pp. 152–166, 2018.

[50] J.-Y. Lee and A. K. Nandi, "Extraction of impacting signals using blind deconvolution," *J Sound Vib.,* vol. 232, pp. 945–962, 2000.

[51] J. Antoni, "The spectral kurtosis: A useful tool for characterising non-stationary signals," *Mech Syst Signal Process.,* vol. 20, pp. 282–307, 2006.

[52] S. Schmidt, P.S. Heyns, and K.C. Gryllias, "An informative frequency band identification framework for gearbox fault diagnosis under time-varying operating conditions," *Mech Syst Signal Process.,* vol. 158, p. 107771, 2021.

[53] B. Hou, D. Wang, J.-Z. Kong, J. Liu, Z. Peng, and K.-L. Tsui, "Understanding importance of positive and negative signs of optimized weights used in the sum of weighted normalized Fourier spectrum/envelope spectrum for machine condition monitoring," *Mech Syst Signal Process.,* vol. 174, p. 109094, 2022.

[54] T. Yan, D. Wang, M. Zheng, C. Shen, T. Xia, and Z. Peng, "Interpretable sparse learned weights and their entropy based quantification for online machine health monitoring," *Mech Syst Signal Process.,* vol. 199, p. 110493, 2023.

[55] M. E. Tipping and C. M. Bishop, "Probabilistic principal component analysis," *J R Stat Soc Series B Stat Methodol.,* vol. 61, pp. 611–622, 1999.

[56] D. N. Wilke, P. S. Heyns, and S. Schmidt, "The role of untangled latent spaces in unsupervised learning applied to

condition-based maintenance," In A. Hammami, P.S. Heyns, S. Schmidt, F. Chaari, M.S. Abbes, M. Haddar (Eds.), *Modelling and Simulation of Complex Systems for Sustainable Energy Efficiency,* New York: Springer International Publishing, 2022: pp. 38–49.

[57] C. M. Bishop, "Pattern recognition and machine learning," 1st ed., New York: Springer, 2006.

[58] D. P. Kingma and M. Welling, "Auto-encoding variational Bayes," 2013. http://arxiv.org/abs/1312.6114.

[59] A. Hyvärinen and E. Oja, "Independent component analysis: algorithms and applications," *Neural Netw.,* vol. 13, pp. 411–430, 2000.

[60] A. Hyvarinen, "Fast and robust fixed-point algorithms for independent component analysis," *IEEE Trans Neural Netw.,* vol. 10, pp. 626–634, 1999.

[61] P. Comon, "Independent component analysis, a new concept?," *Signal Process.,* vol. 36, pp. 287–314, 1994.

[62] S. Braun and B. Seth, "Analysis of repetitive mechanism signatures," *J Sound Vib.,* vol. 70, pp. 513–526, 1980.

[63] J. Antoni and R. B. Randall, "The spectral kurtosis: Application to the vibratory surveillance and diagnostics of rotating machines," *Mech Syst Signal Process.,* vol. 20, pp. 308–331, 2006.

[64] I. J. Goodfellow, J. Pouget-Abadie, M. Mirza, B. Xu, D. Warde-Farley, S. Ozair, A. Courville, and Y. Bengio, "Generative adversarial nets," in: Adv Neural Inf Process Syst, 2014. https://proceedings.neurips.cc/paper/2014/file/5ca3e9b122f61f8f06494c97b1afccf3-Paper.pdf.

[65] W. Hu, T. Wang, and F. Chu, "A Wasserstein generative digital twin model in health monitoring of rotating machines," *Comput Ind.,* vol. 145, p. 103807, 2023.

[66] D. Marx and K. C. Gryllias, "Domain knowledge informed unsupervised fault detection for rolling element bearings," *PHM Society European Conference.,* vol. 7, pp. 338–350, 2022. https://doi.org/10.36001/phme.2022.v7i1.3348.

[67] D. S. Broomhead and G. P. King, "Extracting qualitative dynamics from experimental data," *Physica D.,* vol. 20, pp. 217–236, 1986.

[68] M. E. Wall, A. Rechtsteiner, and L. M. Rocha, "Singular value decomposition and principal component analysis," in: *A Practical Approach to Microarray Data Analysis,* Boston: Springer, 2002.

[69] X. Zhao and B. Ye, "Similarity of signal processing effect between Hankel matrix-based SVD and wavelet transform and its mechanism analysis," *Mech Syst Signal Process.,* vol. 23, pp. 1062–1075, 2009.

[70] E. Bozzo, R. Carniel, and D. Fasino, "Relationship between singular spectrum analysis and Fourier analysis: theory and application to the monitoring of volcanic activity," *Computers and Mathematics with Applications.,* vol. 60, pp. 812–820, 2010.

[71] M. Zhao and X. Jia, "A novel strategy for signal denoising using reweighted SVD and its applications to weak fault feature enhancement of rotating machinery," *Mech Syst Signal Process.,* vol. 94, pp. 129–147, 2017.

[72] Y. Chen, X. Liang, and M. J. Zuo, "An improved singular value decomposition-based method for gear tooth crack detection and severity assessment," *J Sound Vib.,* vol. 468, p. 115068, 2020.

[73] R. Golafshan and K. Yuce Sanliturk, "SVD and Hankel matrix based de-noising approach for ball bearing fault detection and its assessment using artificial faults," *Mech Syst Signal Process.,* vol. 70–71, pp. 36–50, 2016.

[74] Q. He, Z. Feng, and F. Kong, "Detection of signal transients using independent component analysis and its application in gearbox condition monitoring," *Mech Syst Signal Process.,* vol. 21, pp. 2056–2071, 2007.

[75] A. Hyvärinen, J. Karhunen, and E. Oja, "*Independent Component Analysis,*" New York, USA: John Wiley & Sons, Inc., 2001.

[76] M. E. Davies and C. J. James, "Source separation using single channel ICA," *Signal Process.,* vol. 87, pp. 1819–1832, 2007.

[77] R. Balshaw, P. S. Heyns, D. N. Wilke, and S. Schmidt, "A spectral regularisation framework for latent variable models designed for single channel applications," 2024.

[78] S. Mohamed and B. Lakshminarayanan, "Learning in implicit generative models," 2016. http://arxiv.org/abs/1610.03483.

[79] J. Ho, A. Jain, and P. Abbeel, "Denoising diffusion probabilistic models," Adv Neural Inf Process Syst 2020-Decem. 2020, 1–25.

[80] D. M. Blei, "Build, compute, critique, repeat: data analysis with latent variable models," *Annu Rev Stat Appl.,* vol. 1, pp. 203–232, 2014.

[81] D. M. Blei, A. Kucukelbir, and J. D. McAuliffe, "Variational inference: a review for statisticians," *J Am Stat Assoc.,* vol. 112, pp. 859–877, 2017.

[82] C. Cremer, X. Li, and D. Duvenaud, "Inference suboptimality in variational autoencoders," 2018, 1–14. http://arxiv.org/abs/1801.03558.

[83] K. Preechakul, N. Chatthee, S. Wizadwongsa, and S. Suwajanakorn, "Diffusion autoencoders: Toward a meaningful and decodable representation," In *IEEE Conference on Computer Vision and Pattern Recognition (CVPR),* New York City: IEEE, 2022.

[84] A. Hyvärinen, "New approximations of differential entropy for independent component analysis and projection pursuit," *Adv Neural Inf Process Syst.,* vol. 10, pp. 273–279, 1998.

[85] N. Sawalhi, "The application of spectral kurtosis to bearing diagnostics," in: Acoustics - Conference, 2004: pp. 393–398. http://www.acoustics.asn.au/conference_proceedings/AAS2004/ACOUSTIC/PDF/AUTHOR/AC040115.PDF.

[86] O. Surucu, S. A. Gadsden, and J. Yawney, "Condition monitoring using machine learning: A review of theory, applications, and recent advances," *Expert Syst Appl.,* vol. 221, p. 119738, 2023.

[87] H. Qiu, J. Lee, J. Lin, and G. Yu, "R.T. Services (2007), IMS, University of Cincinnati. Bearing Data Set, NASA Ames Prognostics Data Repository," 2007. http://ti.arc.nasa.gov/project/prognostic-data-repository.

[88] W. Gousseau, J. Antoni, F. Girardin, and J. Griffaton, "Analysis of the rolling element bearing data set of the center for intelligent maintenance systems of the University of Cincinnati," in: 13th International Conference on Condition Monitoring and Machinery Failure Prevention Technologies, 2016. https://hal.science/hal-01715193/file/216-Gousseau.pdf.

[89] M. Feldman, "Hilbert transform in vibration analysis," *Mech Syst Signal Process.,* vol. 25, pp. 735–802, 2011.

[90] S. Schmidt, A. Mauricio, P. S. Heyns, and K. C. Gryllias, "A methodology for identifying information rich frequency bands for diagnostics of mechanical components-of-interest under time-varying operating conditions," *Mech Syst Signal Process.,* vol. 142, p. 106739, 2020.

[91] D. W. Hogg, "Data analysis recipes: Probability calculus for inference," 2012. http://arxiv.org/abs/1205.4446.

[92] T. Y. Lee, J. V. Zidek, and N. Heckman, "Dimensional analysis in statistical modelling," 2020. http://arxiv.org/abs/2002.11259.

[93] S. Schmidt, R. Zimroz, F. Chaari, P. S. Heyns, and M. Haddar, "A simple condition monitoring method for gearboxes operating in impulsive environments," *Sensors,* vol. 20, p. 2115, 2020.

[94] H. Hotelling, "Analysis of a complex of statistical variables into principal components.," *J Educ Psychol.,* vol. 24, pp. 417–441, 1933.

[95] D. Wang, "Some further thoughts about spectral kurtosis, spectral L2/L1 norm, spectral smoothness index and spectral Gini index for characterizing repetitive transients," *Mech Syst Signal Process.,* vol. 108, pp. 58–72, 2018.

APPENDIX A

RELATIONSHIP TO SIGNAL PROCESSING

This section demonstrates a simple connection between existing signal processing work and the considered PCA-based and negentropy-based ICA methods used in this work. The purpose is to detail the characteristics of the observed data that the considered methods extract and highlight. This is important to the online training approach as the LVMs extract information dynamically through record time, responding to recorded data changes based on their specific characteristics of interest.

The PCA objective function can be given as

$$\max_{\boldsymbol{u}_j} \mathcal{L}_{\text{PCA}}(\boldsymbol{u}_j) = E_{\boldsymbol{x}\sim p(\boldsymbol{x})}(\boldsymbol{u}_j^T\boldsymbol{x})^2 \quad s.t.\, \boldsymbol{u}_j^T\boldsymbol{u}_k = \delta_{jk}, \tag{29}$$

where δ_{ij} represents the Kronecker delta function, and $\boldsymbol{x}$ is assumed to be pre-processed using Equation (11). The PCA represents the maximization of the variance of the j^{th} projection of the data $\boldsymbol{x}$, i.e., the j^{th} latent variable [94]. The PCA objective can be reformulated into a Rayleigh quotient function $R(\boldsymbol{C},\boldsymbol{x})$ for the symmetric covariance matrix $\boldsymbol{C}$ and can be solved as an eigenvalue problem or via the singular value decomposition of $\bar{\boldsymbol{X}}$ obtained using Equation (11) [57].

The negentropy-based ICA objective function can be represented as

$$\max_{\boldsymbol{w}_j} \mathcal{L}_{\text{ICA}}(\boldsymbol{w}_j) = J(z_j) \approx c\cdot(E_{\boldsymbol{x}\sim p(\boldsymbol{x})}\{G(\boldsymbol{w}_j^T\boldsymbol{x})\} - E_{\nu\sim p(\nu)}\{G(\nu)\})^2 \quad s.t. \boldsymbol{w}_j^T\boldsymbol{w}_k = \delta_{jk}, \tag{30}$$

where $J(z_j)$ is the negentropy of the j^{th} latent component, $G(\cdot)$ is a non-quadratic function, $c \in R^+$ is an arbitrary constant, $\nu \sim \mathcal{N}(0,\sigma_\nu^2)$ is a standardized Gaussian variable with variance $\sigma_\nu^2 = E_{z\sim p(z_j)}\{(z - E\{z\})^2\} = \sigma_{z_j}^2$, and $\boldsymbol{x}$ is pre-processed using Equation (11) and Equation (12). This objective function is presented in Hyvärinen [65]. A fixed-point algorithm called FastICA was proposed to estimate $\boldsymbol{W}$ [75].

The implication of the data Hankelization step in Equation (10) for the considered online LVMs, for the case where $L_{sft} = 1$, is that the SRICA and PPCA component vectors operate as a set of finite impulse response (FIR) filters [75,76]. This demonstrates the strong correlations between the LVMs used in this work and known signal processing-based methodologies. First, consider the PCA objective function given in Equation (29). It is trivial to show, for vibration-based applications, that the optimal solution for Equation (29) can be reformulated into

$$\mathcal{L}_{\text{PCA}}(\boldsymbol{u}_j) = \boldsymbol{u}_j^T\boldsymbol{C}\boldsymbol{u}_j = E\{z_j^2\} = \lambda_j, \tag{31}$$

where the covariance matrix $\boldsymbol{C} = \frac{1}{N}\bar{\boldsymbol{X}}^T\bar{\boldsymbol{X}}$ also represents the auto-correlation matrix, $(\lambda_j,\boldsymbol{u}_j)$ is the j^{th} eigenpair that diagonalizes $\boldsymbol{C}$ and $E\{z_j^2\}$ represents the power of the j^{th} latent signal. In this setting, the PCA objective seeks to maximize the power of the filtered signal, and $\boldsymbol{u}_j$ is an FIR filter driven to capture components with maximal power.

Secondly, consider the ICA objective function given in Equation (30). It is trivial to show that for the choice $G(u) = u^4$ Equation (30) becomes

$$\mathcal{L}_{ICA}(\boldsymbol{w}_j) = (E\{z_j^4\} - E\{\nu^4\})^2 = \left(E\left\{\left(\frac{z_j - \mu_{z_j}}{\sigma_{z_j}}\right)^4\right\} - 3\cdot\sigma_\nu^4\right)^2 = (\text{kurt}(z_j) - 3)^2, \tag{32}$$

where $\mu_{z_j} = 0$ and $\sigma_{z_j} = 1$ as the data is assumed to be centered and whitened, and c = 1. This represents the square excess kurtosis of latent component z_j. Hence, the ICA objective seeks to maximize the non-Gaussianity of the filtered signal by maximizing its kurtosis, or a generalization thereof, and $\boldsymbol{w}_j$ operates as an FIR filter that captures the dominant non-Gaussian components of the signal. Hence, it is shown that online LVM methodologies represent fundamentally different latent manifolds, and the learnt latent components capture the sources of maximal power or non-Gaussianity. However, unlike blind deconvolution [34] or band demodulation [33] methodologies, which seek a single transformation, i.e., $d = 1$, that maximizes some measure, e.g., the L2/L1 norm [95], the considered linear LVMs seek d latent variables, i.e., d latent transformations that capture the intrinsic features of observed data in alignment with their objective functions on the condition that the sources be statistically independent.